I. Design of Double Cone for Experimentation on Shock and Boundary Layer Interaction

II. Mars Science Laboratory Heat Flux Measurements in T5 Hypervelocity Shock Tunnel Facility

Matthew G. Leibowitz

Jean-Christophe Veilleux

Nelson J. Yanes

Experimental Methods

Ae 104 C

California Institute of Technology

Pasadena

06-04-2015

1 Acknowledgments

The authors would like to recognize the overwhelming support of members of the hypersonics group and the machine shop of GALCIT. The entirety of the project would not be possible without the input of Joe Haggerty and Ali Kiani, who often worked after-hours to fabricate challenging parts with complex geometry. Whenever questions are left unanswered or issues arise, Bahram Valiferdowsi was always there to assist the team in times of need. His experience in working in T5 was paramount for the quality of the experiments we performed. The excellent data we have obtained is all a result of Bahram's guidance. Always found upstairs in T5, Andrew Knisely and Bryan Schmidt provided excellent advice and consultation. When the time came to run an experiment in T5, Andrew and Bryan dropped their work and assisted us in going through the preparation check list. A huge thanks to Professor Hans Hornung, whose years of expertise in hypersonic flow was crucial in understanding the physics of the problem at hand. A final thanks must be given to Professor Joanna Austin, whose guidance and expertise in the project made it possible to complete not just one but two projects in a short period of time. The authors are deeply fortunate to have the help of the mentioned names above.

Contents

2 Introduction

Two projects were completed under the fulfillment of Ae104C Experimental Methods. The subsequent report is divided into two parts. First is the design of a double cone model for studying shock and boundary layer interaction. The second part is the testing of a model Mars Science Laboratory heat shield to obtain heat flux data using the T5 Hypersonic Shock tunnel.

2.1 Part I: Design of double cone

Hypersonic flows over double cones are canonical problems where there is a strong coupling between fluid mechanics and thermochemistry. Typically, the reacting flows contain various complex phenomena such as boundary layer separation, shock and shear layer interaction, shock impingement, etc. Computational models are not always able to accurately predict the main features of the flow, and such discrepancies must be resolved. As a result, there has been interest in validating computational models of these problems with experimental results from various facilities. The Hypersonic Expansion Tube (HET), previously at the University of Illinois and recently relocated to Caltech, provided a data set of heat-flux measurements for high enthalpy flow over a double wedge geometry. However, this type of experimentation was not done on double cone geometry, where the main features of the flow are likely to be different due to the three-dimensional geometry. A new double cone model was designed and fabricated as part of a new effort to validate computational models with a new heat flux data set. Experimentation on this new model will also quantify the differences between T5 and other facilities nationwide. The model was designed to be compatible with the T5 reflected shock tunnel facility in order to study shock and boundary layer interaction in hypersonic flow.

2.2 Part II: Mars Science Laboratory heat flux measurements

Following the successful landing of the Mars Science Laboratory's Curiosity rover, valuable data from the hypersonic reentry phase of the vehicle was obtained and compared against aerodynamic predictions. Despite the numerous experimental work conducted by facilities nationwide, discrepancies have been observed between experimental results obtained on the ground and the data recorded during flight. More experimental work is required in order to explain these discrepancies, develop a better understanding of the physics, and gain insights on how to better predict the physics of the flow on a re-entry vehicle. A pre-existing model used for obtaining heat flux measurements in the Hypersonic Expansion Tube was tested in the T5 reflected shock tunnel facility for a number of conditions. A new sting was designed to withstand the intense aerodynamic loads encountered during testing. Heat flux data, as well as chemiluminescence images, were obtained and analyzed. A study of experimental data between other facilities, including the HET, was also conducted.

Part I

Design of Double Cone for Experimentation on Shock and Boundary Layer Interaction

3 Background and motivation

In recent years, a vast number of studies have been performed on shock/shock interaction and shock/boundary layer interaction in hypersonic flow over double wedges or cones. These relatively simple geometric configurations establish very complex and coupled flow phenomena. As a result, these serve as excellent canonical problems to benchmark computational fluid dynamic (CFD) models. The main features of the flow is highlighted in Figure 1 for a particular geometry, where some wave interactions have been omitted for clarity (see Swantek A.B. (2012) for more details). For a particular model configuration, a boundary layer forms and grows in size until a region of flow separation forms. Due to the adverse pressure gradient in this location, a shock forms upstream of the separated region (region 2). This shock interacts with both the attached shock at the leading edge and the bow shock formed by the second cone. In most cone cases, a triple point forms with the intersection of the bow shock and separation shock (Swantek (2012)). Finally, a shear layer separates the hot, slow flow from the bow shock and the fast, cold flow from the reattachment shock when the flow turns in region 3. Depending on the free stream chemistry, flow conditions may vary from this description, making predictions extremely dependent on the thermochemical model.

Numerous numerical and experimental studies have been performed, including those of Swantek (2012), Nompelis (2010), and Holden and Candler. In addition, several comparisons have been made between CFD simulations and experimental results of wall heat flux. A dataset of experimental results has been obtained in the Calspan - University at Buffalo Research Center (CUBRC) Large Energy National Shock (LENS) facility. These experimental results from CUBRC have been compared against CFD predictions to study the discrepancies (see Nompelis (2010)). In addition, Swantek (2012) also conducted several experiments of hypersonic flow over a double wedge geometry with the Hypervelocity Expansion Tube (HET) facility. Heat flux measurements were performed with air and nitrogen as the test gas. It was confirmed through these experiments that gas composition can change the flow conditions and result in different heat flux data for the same stagnation enthalpy.

To date, numerical methods for modeling shock/shock and shock/boundary layer interactions still need significant improvement, particularly for high enthalpy flow conditions. Discrepancies still exist between predicted heat flux and experimental measurements (Nompelis (2010)). In order to mitigate these discrepancies, a better understanding of the physics is necessary to improve upon computational models. This includes using diagnostic tools such as fast-response

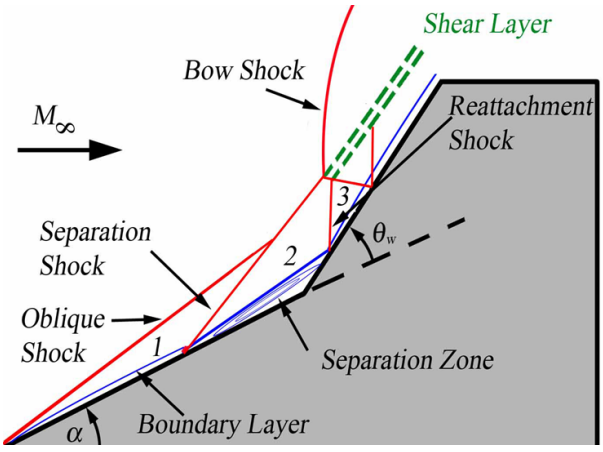

Figure 1: Typical flow features over double cone and double wedge geometries, simplified to highlight important features (reproduced from Swantek A.B. (2012)).

co-axial thermocouples to measure the surface's temperature, and hence compute the heat flux, along with flow imaging, such as schlieren or chemiluminescence, to measure shock geometry.

A new double cone model has been designed and manufactured in order to measure surface heat flux with high spacial resolution using the T5 shock tunnel facility. Dimensions of the double cone were selected to scale a 25° - 55° model used by Swantek (2012) and Nompelis (2010) in order to compare experimental results between facilities. A total of 64 thermocouple locations were placed to study possible three dimensional-effects due to the three-dimensional geometry. The array consists of four groups of 16 thermocouples, each separated by 90°. Each of the four groups consists of two staggered thermocouple arrays that provide a more detailed resolution in the streamwise direction. As a final design feature, a sting was designed to withstand the extreme conditions in the test section and to be compatible with the current T5 setup. It is expected that within the lifetime of the model, a large database of heat flux measurements will be formed in the future.

4 Design of double cone

This section contains a detailed explanation of the design procedure. All computer aided design (CAD) was done using the software *SolidWorks*. As a note, all final machine drawings are compiled in Appendix A for ease of view.

4.1 Geometry

The main geometry of the model consists of a leading edge cone at a 25° inclination angle and a rearward cone at a 55° inclination angle (angles are measured from the axis of symmetry). The intersection of the two cones forms a hinge that sharply turns the flow. The two angles were selected to be matched with the models used by Nompelis (2010) and Swantek A.B. (2012).

In order to ensure compatibility with the T5 test section, the largest outer diameter was selected to match previous aluminum models that have been tested in the past. This prevents the size of the model to be larger than the "clean" free stream of gas at the exit of the nozzle. The largest diameter was selected to be 4.815 inches in length, corresponding to the base length of the 55° cone.

Due to the simple geometry of the model, correct scaling between two double cone models only consists of matching the two inclination angles and the ratio of the two cone's base diameter. For example, the model used by Swantek (2012) has a large diameter of 2.5 inches and a small diameter of 0.984 inches. The ratio of the 55° cone base and the 25° cone base was computed to be approximately 2.54. Because the model of Swantek is a scaled model of Nompelis' model, the ratio of 2.54 was also used in the development of the new model. The base diameter of the 25° cone was selected to be 1.896 inches to satisfy this ratio. Measured from the leading edge tip, the length of the first 25° cone is 2.033 inches. This also sets the second cone to have a length of 1.022 inches. An additional thickness of 1.0 inch was added to the base of the model. This allows enough material to include 6 threaded holes, used with 1/4 inch-20 screws, for mounting the model to the sting.

In order to give enough clearance for mounting thermocouples by hand, the model was hollowed out to a specified shape. To ensure the probes will be correctly positioned during the mounting process, the maximum thickness of the probed regions were constrained to be approximately 3/8 inches. A thicker model will make it difficult to keep the thermocouples flushed with the surface. For ease of machining, the interior of the model was hollowed at three locations. Figure 2 shows a selectional view of the hollowed geometry. A 3.4 inch diameter hole was excavated from the back side of the model at a depth of 1.256 inches. Afterward, two tapered holes were formed to satisfy thickness requirements. Because it is not necessary to have a tapered hole that ends at the tip, a regular hole was simply added to the drawings to match the drill bit used to excavate material. In the final fabrication, the interior of the model was not completely smoothed out at the farthest depth. However, it was not crucial to the project.

4.2 Thermocouple locations

Throughout the design process, the number of thermocouples and their positions have been revised several times. Installing an array of 12 thermocouples that are flush with the surface and completely functional requires approximately 1 week of work to complete. The initial motivation of the project was to only measure heat flux at a maximum of 15 locations using the T5 shock tunnel facility. This would require roughly a week and a half for installing the probes. However, it was decided that more thermocouples will allow more redundancy and resolution

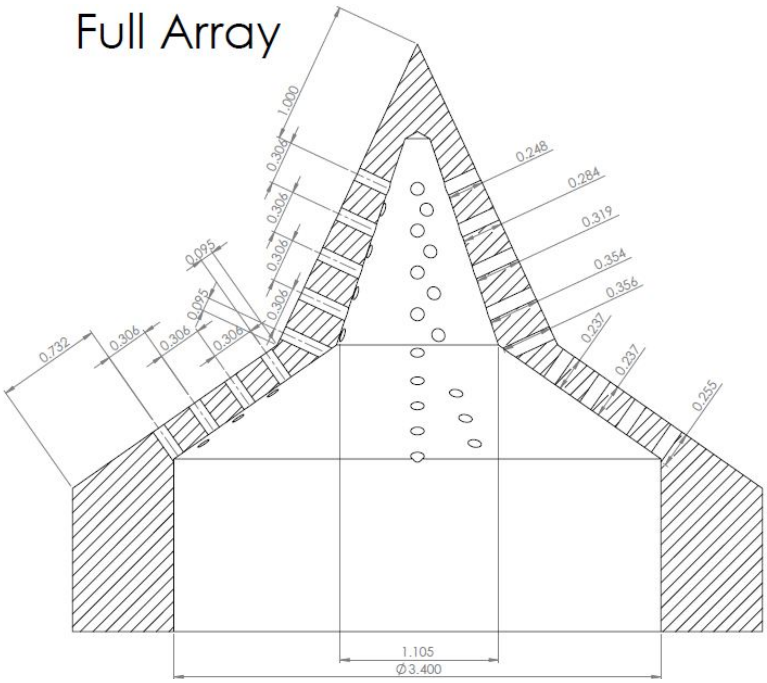

Figure 2: Cross sectional view of the model with hole locations and depths visible early in the design stage.

in the collected data. T5 requires excellent maintenance for continuous operation. Any major damage to the tunnel can substantially force the facility to be inoperable for several days, losing precious testing time. Including additional thermocouples can increase the data set for every high risk shot. Finally, the lifetime of the model is limited by the number of tests performed. In the past, debris from the main diaphragm have damaged the surface finish of the model, causing intense scaring in soft metals. As a result, the number of thermocouples increased to 64.

Figure 3 shows the final thermocouple configuration of the model. The 64 thermocouples are divided into four formations. Each formation consists of two lines of thermocouples in the streamwise direction. This provides 16 heat flux measurements for the flow described in the background and motivation section. Each of the four leading edge thermocouples is located 1 inch from the tip (measured along the surface in the streamwise direction). From experimental results on double wedges by Swantek (2012), it was found that the separated region occurs approximately after x/L=0.6. Since we are more interested in understanding the separation region, there is no need to put thermocouples closer to the tip.

One line consists of 5 thermocouples on the 25° cone and 4 thermocouples in the 55° cone. In order to measure heat flux in the region next to the hinge, two of these probes are placed next to the intersection of the two cones. A second line of staggered thermocouples is placed at a 15 degree offset relative to the first line. This offset angle was selected to be close enough to the first array, but have enough material between the probes to be structurally sound. The second line contains an additional 4 thermocouples on the 25° cone and 3 thermocouples on the 55° cone. This staggered line of probes increases the resolution of the heat flux measurements.

There are two advantages in repeating each formation four times at 90° intervals. First, this allows redundancy in the data set. For every test in T5, 4 complete measurements at each spanwise location can be obtained and analyzed. Secondly, it is possible to observe any three-dimensional effects in the flow field by studying the correlation between thermocouples. For example, if the free stream flow is not uniform due to the orientation of the probe, it is

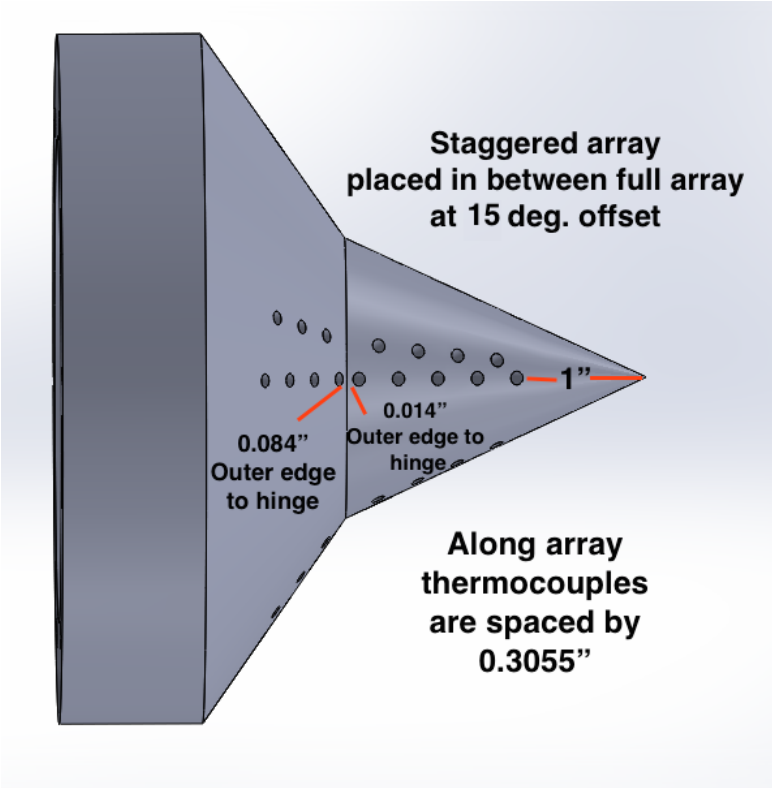

(a) A detailed view of two thermocouple rows that forms each of the four formations.

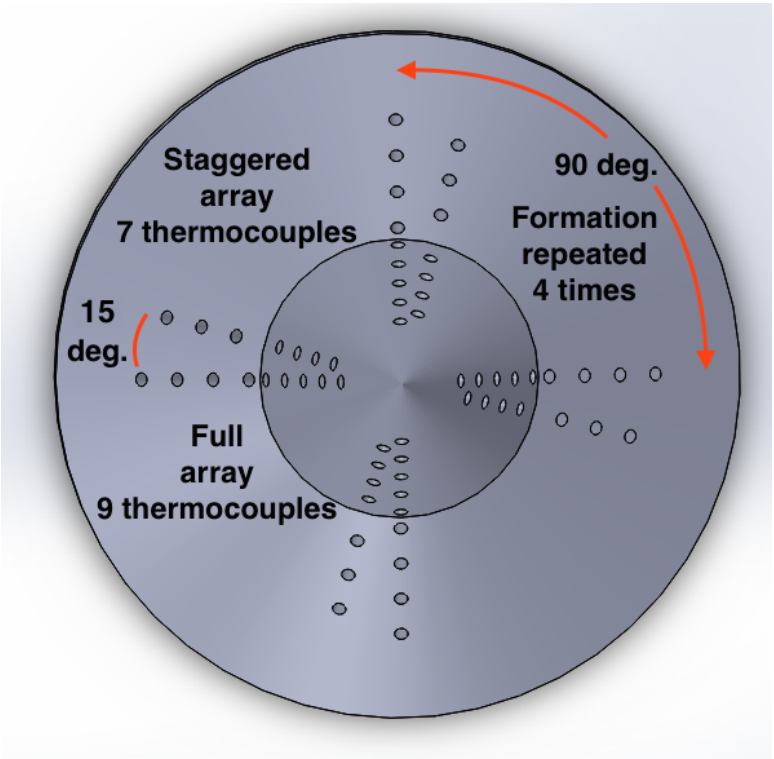

(b) Front view of thermocouple orientations.

Figure 3: Final thermocouple locations for double cone model.

possible to study the changes in heat transfer on opposing arrays.

4.3 Sting

Mounting the model inside of the test section is accomplished by using clamps that secure a 2 inch outer-diameter pipe. To attach the model to the pipe, a flange was designed, manufactured and welded to the pipe. On the other side of the welded flange, a register is machined to mate with the backside of the double cone. To secure the model, 6 screws are tightened to join the model and the flange. All thermocouple cables are fed through the hollow pipe, into a feed tube that eventually connects to the data acquisition system.

4.4 Material

The entire model was specified to be A2 tool steel. Although more difficult to machine than aluminum, this higher strength material was selected to increase the life time of the model in the laboratory. As mentioned previously, past aluminum models suffered from surface scarring from debris in the test section. Over time, these models became unusable. The steel material is expected to perform better than aluminum.

5 Fabrication

Completion of the initial design was done in one week, a task that was proved challenging to machinists. After the design was complete, a small error in the dimension of the small diameter caused the team to rework the design. In order to increase the diameter ratio to 2.54, some thickness on the 25° cone was removed to reduce the smaller diameter. Once the solution was found, the final model contained the correct inclination angles and diameter ratio. A tip radius of 1×10^{-4} inches was specified. Figures 4 and 5 show images of the final model. Figure 6 shows the final manufactured sting.

Figure 4: Side view of completed double cone model with two thermocouple groups visible.

Figure 5: Front view of model with all 64 thermocouple locations visible.

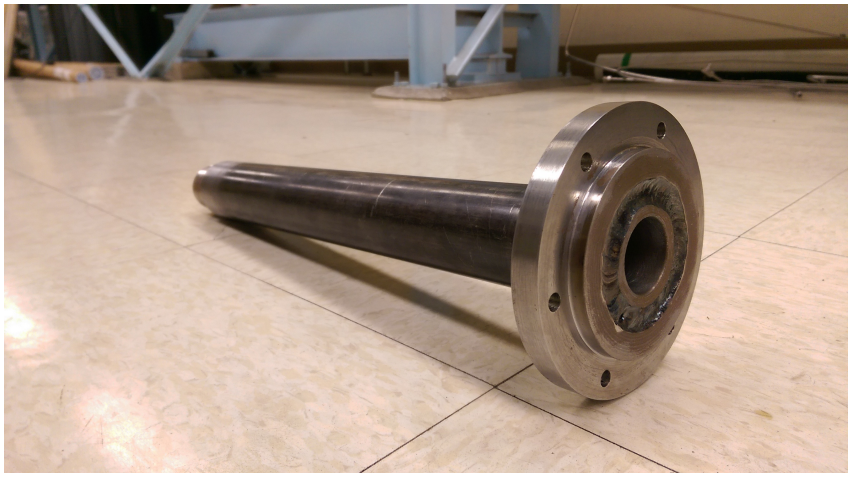

Figure 6: Final sting assembly.

6 Partial conclusion

A new model was successfully developed for studying shock/shock and shock/boundary layer interaction in the T5 hypersonic shock tunnel facility. In addition, components for mounting the model are available for researchers. The final model is an exact scaled version of the models used by Swantek A.B. (2012) and Nompelis (2010). In addition, it is expected to have a long lifetime in T5. Once all thermocouples are mounted, this probe will provide several data sets for validating CFD simulations in the current literature.

The completion of this model marked a turning point in our Ae104C project. It was decided that there was not enough time to install all thermocouples and proceed with the experimental phase. As a result, a second project was selected.

Part II

Mars Science Laboratory Heat Flux Measurements in T5 Hypervelocity Shock Tunnel Facility

7 Background

The successful landing of the 2012 Mars Science Laboratory (MSL) *Curiosity* rover was made possible by the complex entry, descent, and landing architecture. This was an impressive feat that utilized an aeroshell, a blunt body casing surrounding the rover, to protect it during the hypersonic CO_2 atmospheric entry into Mars.

While this was an incredible accomplishment, to be capable of launching higher mass vehicles for robotic sample return and human exploration to Mars, improved accuracy in the prediction of aerodynamics and thermal loads must be made. According to the NASA Entry, Descent, and Landing Roadmap of Technology Area 09, current estimates on the extensibility of the MSL architecture indicate that it is limited to roughly 1.5 tons delivered mass without significant investments in new technologies. Human scale mass missions, the ultimate goal in NASA's human space exploration plans, will require 20-60 tons of landed payload mass (Adler (2010)).

These upcoming missions will require an improved understanding of the interaction of thermal transitions and chemical reactions within the flow field. Currently, the Mars Science Laboratory (MSL) carries up to 50% uncertainty on the predicted turbulent heating levels (Edquist and C.Y. (2007)). The deficiencies in our understanding of non-equilibrium flows, such as in the Martian CO_2 atmosphere during reentry, have practical design consequence. The heat shield for MSL was designed based on computational models that predicted a super catalytic (100% recombination) wall boundary condition. While this was a conservative approach validated through ground testing, there are reasons to believe there are a lot of uncertainties in the experiments (Hollis (2013)).

Such a situation is unacceptable, and there is a need to produce experimental validation through ground testing. Current state-of-the-art simulations are limited by a lack of experimental data, and the free-stream thermochemical state is not well characterized for the experimental data available. According to Hollis (2013), "reduction of the modeling uncertainties will require the acquisition of new, high-fidelity experimental ground-test and flight-test data on both macroscopic aerothermodynamics properties (surface heating and pressure, flow-field structure, aerodynamics forces and moments, boundary-layer transition, etc.) and fundamental physical properties (chemical, vibrational, and electronic excitation and relaxation rates, transport properties, and radiation emission and absorption rates)."

The work for this project was designed to compare MSL data from different high enthalpy ground testing facilities to new data from the Caltech T5 reflected shock tunnel (now with the contoured nozzle having a 100:1 throat area ratio). Previous MSL studies have been completed in the NASA Ames 42-Inch shock tunnel, The GASL HYPULSE expansion tunnel, the CUBRC LENS I and LENS X reflected shock tunnel and expansion tunnel, a previous experiment in the Caltech T5 reflected shock tunnel with a different nozzle and the Hypervelocity Expansion Tube (HET) previously at the University of Illinois and now at Caltech. The survey of ground test data done by Hollis (2013) could not specify any specific test runs that produced reliable laminar, aeroheating in high enthalpy, carbon dioxide flow. This is due to discrepancies and uncertainties in the experiments such as free stream condition specification, catalytic behavior, and interpretation of the data.

The goal will be to gather heat flux and standoff shock distance in order to create a new dataset in which to help validate computational models. The data will be compared to different facilities to try to collapse and compare data. Previous attempts to compare results from different facilities have proven to be challenging as the free stream parameters can vary drastically, because the ways of creating high enthalpy flow in the different facilities are vastly different.

8 Redesign of the MSL-sting

The decision was made to test the MSL model previously tested in the Hypervelocity Expansion Tube (HET) in the T5 reflected shock tunnel. The model can be seen on the sting used in the HET in Figure 7. At first, consideration was given into using the existing sting in the T5 Reflected Shock Tunnel. Since T5 produces different free stream conditions in the test section and thus over the model, an analysis of the forces produced on the rod was done to see if it can survive in T5. As a first estimation, given the current nozzle, the density is approximately 10 times higher in the T5 facility than it is in the HET, so the loads on the model will be approximately 10 times higher as well.

First, the dynamic pressure in the free stream was found using modified newtonian flow theory developed by former Caltech professor Lester Lees (Braun (2014)). According to this theory, the coefficient of pressure is valid for hypersonic flows where the Mach number is high (good approximation when M>5) and equal to:

$$C_p \;=\; C_{p,max}\, Cos(\delta)^2 \;. \tag{1}$$

The dynamic pressure is then given by:

$$\frac{C_p\, \rho_\infty U_\infty^2}{2} \;, \tag{2}$$

where ρ_∞ and U_∞ are respectively free stream density and velocity. At this stage, a test condition had not been selected for the experimental phase. Instead, a representative test condition from the T5 Conditions Report (Jewell and Shepherd (2014)) was used where the free stream is typically $\rho_\infty = 0.1$ kg/m^3 and $U_\infty = 2500$ m/s.

According to Braun (2014), a common approximation for a CO_2 (martian) atmosphere free stream is $\gamma = 1.3$ and $C_{p,max} = 1.869$. δ is given by the angle of attack of the model which is 16° for our test conditions. An angle of attack of 16° was chosen to match the average approximate angle that MSL went through the Martian atmosphere and to match the angle of attack from data taken from other high enthalpy ground test facilities. The most recent paper publishing ground test data came from MacLean et al. (2015) where data was gathered in an expansion tube only at a 16° angle of attack. The dynamic pressure in the free stream was estimated to be

$$\frac{1.869\ \cos(16^\circ)^2\ 0.1\ 2500^2}{2} = 539,688\ \text{Pa} \;. \tag{3}$$

The previous sting was then tested to see if it could survive in the T5 facility. The weakest point will be at the base of the rod where the moment produced from the model at an angle of attack will be highest. Using finite element analysis (FEA) on a CAD model of the rod, this moment was reproduced. Since T5 is an impulse facility, the dynamic pressure felt on the model should be multiplied by a factor of 2.5 to estimate the impulse shock loading. An additional factor of safety of 4 was included to be conservative and ensure the sting will not fail. Therefore a pressure of $4{\times}2.5{\times}539688 = 5,396,880$ Pa, or 5.4 MPa, was used as a conservative worst case scenario pressure the model and sting will feel.

The FEA was done using *Autodesk Inventor*. The dynamic pressure was assumed to be distributed on the face of the MSL 2" diameter model with an area of $A = \pi\ D^2/4$. Given a 16° angle of attack, the forces the model would feel from the free stream under the conservative loading are $F_x = PA\cos(\delta) = 2376.2$ lb-force in the x direction (shear force) and

$F_y = PA\sin(\delta) = 681.4$ lb-force in the y-direction (axial loading). Since the rod is the most likely part to break under high loads, this piece was tested first. From the FEA (see Figure 8), the rod will feel a maximum stress of 1000 MPa at the base. According to Engineering Toolbox, grade 8 steel, the material of the rod, has a proof strength of 827 MPa. As a result, permanent deformation is likely to occur.

The decision was then made to redesign the existing sting to safely test the MSL model in the higher dynamic pressure. Requirements of the new sting included a 16° angle of attack to match previous data. This angle of attack piece would be attached to a 2 inch outer diameter rod used to clamp the model into the T5 test section. A locking nut would be used to ensure the line of thermocouples would lined up vertically, normal to the angle of attack. Finally, it was important to avoid feedback effects from the sting onto the surface of the model to ensure the data gathered isn't effected by the sting.

The final design was completed using *Solidworks* and can be seen in Figure 9. The design consists of 7 parts. The machine drawings for each part can be found in Appendix B. The MSL (Figure 23) and MSL aftbody (Figure 24) were previously fabricated and tested in the HET. A register on the MSL aftbody was created to have it sit in the forebody and create a strong fit between the two parts.

A 10 inch long pipe (Figure 29) was needed to clamp the model into the test section of T5. NPT threads were placed on both sides of the pipe. One thread was needed to connect to the plumbing and hose to feed the thermocouples out of the test section. The other thread was created to connect to the incline mount of angle of attack adapter (Figure 26). This piece is a cylinder piece that is cut so the MSL strut (Figure 25) can sit flush on the end at a 16° angle and be screwed in using 6 1/4"-20 screws. The MSL strut is needed to keep the model far enough from the sting to avoid feedback effects. A high strength grade 8 steel rod (Figure 28) is used to connect the strut to the aftbody. The threaded cylinder nut (Figure 27) was created instead of simply using a bolt because the cylinder can be custom made to a larger diameter for greater strength and support. Each of these pieces have a hole drilled through the center to allow the thermocouple wires to pass through.

The sting assembly was tested using finite element analysis where the same loads (2376.2 lb-force in the x direction (shear force) and 681.4 lb-force in the y-direction (axial loading)) were applied, this time on the face of the MSL model. The FEA (Figure 10) shows a maximum estimated stress of 225 MPa. The parts manufactured were then chosen to be made out of 1045 Medium Carbon Steel which has a yield strength of 310 MPa. Since the worst case stress was 85 MPa below yield, the sting could confidently be mounted in T5 without worrying about failure. Also from Figure 10, the deflections are exaggerated and the maximum deflection was estimated to be 0.0047 inches. The GALCIT machine shop manufactured the pieces and the result can be seen in Figure (11).

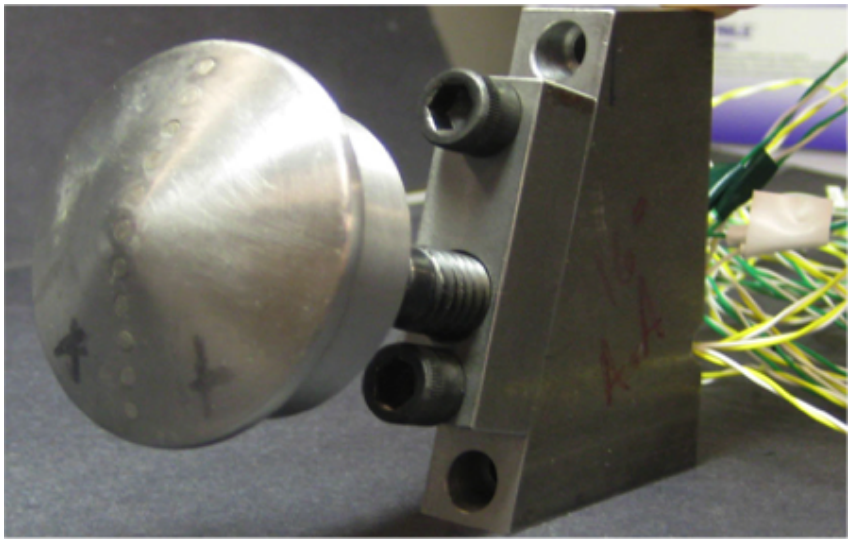

Figure 7: MSL model attached to the sting used in the HET. Model diameter is 2 inches.

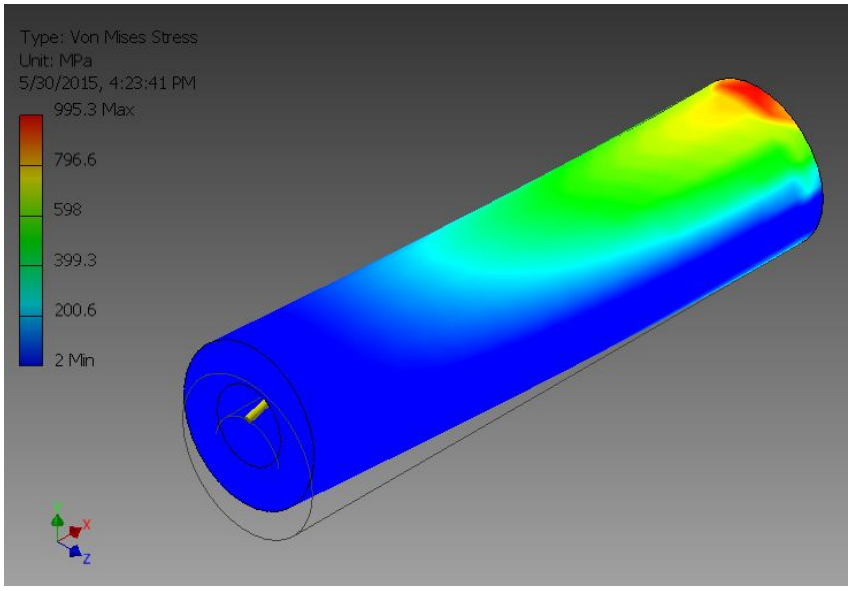

Figure 8: Finite element analysis of the MSL HET rod given a conservative loading from the T5 reflected shock tunnel.

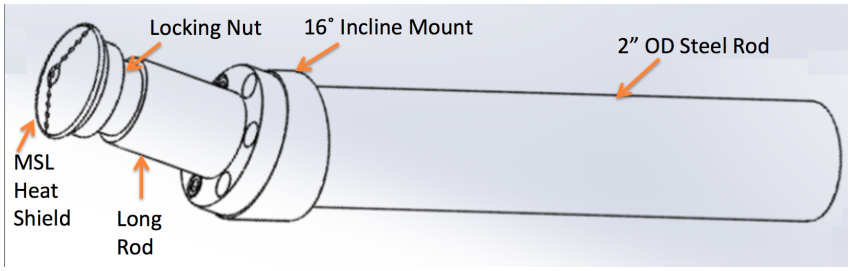

Figure 9: Solidworks assembly of the sting final design.

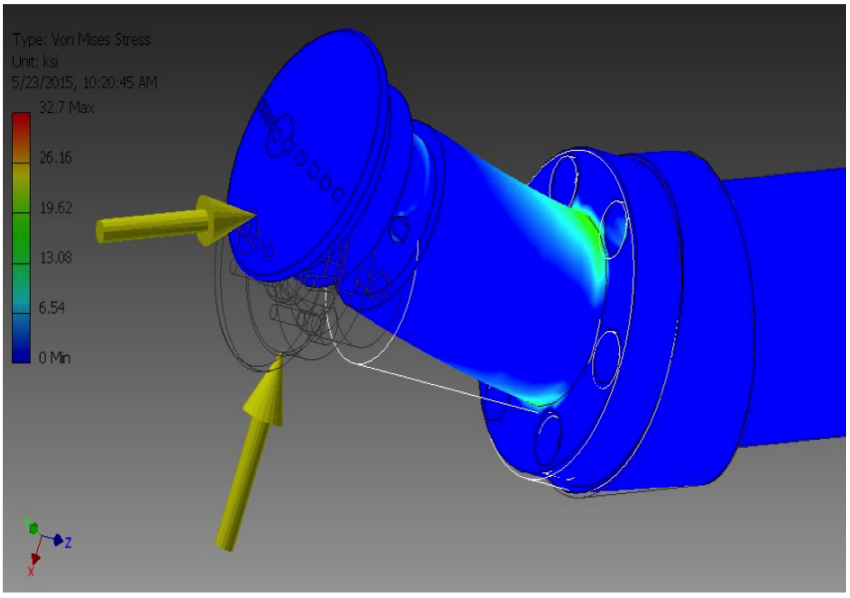

Figure 10: Finite element analysis on the redesigned sting showing maximum loads and deflections under worst case scenario.

Figure 11: MSL model attached to the sting used in the T5 testing.

9 Selection of the test conditions

As one of the objectives of this project is to compare the results obtained using the T5 reflected shock tunnel facility with those obtained using the HET expansion tube, the test conditions have to be carefully chosen in the interest of obtaining a good match. Obviously, matching all freestream parameters between HET and T5 is strictly out of reach. Instead, it is possible to consider some simple equations which have been used in the past for the sake of predicting heat fluxes at surfaces exposed to hypersonic flows, and gain physical insights in the interest of highlighting the key parameter that should be matched.

The simplest possible idea is to consider the freestream flux of energy. From elementary physics, this flux is known to be $\rho_\infty U_\infty^3/2$, where ρ_∞ is the density of the freestream flow, and U_∞ is the freestream velocity. Although this approach is overly simplistic, one could expect the heat flux at the surface of the model to have some sort of dependence upon this energy flux. This teaches us that the heat flux could depend on the third power of the velocity, thus suggesting that matching the velocity is crucial.

A refinement of this simple idea is to consider early correlations which have been successfully used in the past to predict the heat flux at a stagnation point. In general, the stagnation point heat flux can be estimated as:

$$q_w \;=\; C\rho_\infty^{0.5}\, U_\infty^3\, R^{-1/2} \left(1 - \frac{h_w}{h_0}\right) \;, \tag{4}$$

where C is a constant, R is the radius of the nose, h_w is the wall enthalpy and h_0 is the total enthalpy (see Anderson (2006) and Braun (2014) for more details).

Because h_w is expected to be much smaller than h_0 in the present study[1], the term between parentheses in the equation can be approximated as 1. This teaches us, once again, that the wall heat flux should depend on the third power of the velocity. As a result, one could believe that having a match of the freestream velocity is very important for the sake of matching and/or comparing the wall heat flux obtained using different facilities capable of generating hypersonic flows.

The key parameters of the test conditions used in HET are reported in Table 1. Because the calculated[2] freestream velocity of the HET experiment is 3059 m/s (see Sharma et al. (2010)), the selected test condition in T5 should yield approximately the same velocity. Further, the initial composition of the gas in the shock tube has to match the one used in HET, i.e. 100% of CO_2. This is a requirement if one wants to replicate accurately the Martian atmosphere, which roughly consists of 95% of CO_2, the majority of the other 5% is composed of various inert gas.

The test conditions reported by Jewell and Shepherd (2014) have been used in order to select a preexisting test condition for T5. Because very little time was available, designing a new test condition was out of reach, and repeating a previous T5 shot was the best option available. Shot 2723, performed in 2012, used a shock tube composition of 100%, and had a calculated freestream velocity of roughly 3050 m/s. This is the best possible velocity match that could be achieved based on past T5 conditions which used the same nozzle as the one currently installed in the shock tunnel (contoured nozzle with a ratio of 100:1)[3]. More parameters related to shot 2723 are reported in Table 2. Although there is a very good velocity match between the HET

[1] The experiment will be conducted with a cold model at roughly 300 K, and the stagnation enthalpy will be in excess of 5 MJ/kg.

[2] For both HET and T5, the freestream velocity is obtained through CFD (i.e., it is an approximate calculated value and not a measured quantity).

[3] Replacing the nozzle of T5 was not an option due to the short duration of the project.

Table 1: Key parameters characterizing the freestream flow in the HET experiment where the heat fluxes at the surface of the MSL model have been studied (see Sharma et al. (2010)).

Measurement	Symbol	Value	Units
Mach number	M	5.7	—
Velocity	U_∞	3059	m/s
Stagnation enthalpy	Δh_0	5.66	MJ/kg
Static temperature	T_∞	1172	K
Density	ρ_∞	0.014	kg/m^3
Unit Reynolds number	Re_∞	1×10^6	1/m

Table 2: Key parameters characterizing the freestream flow of shot 2723 in T5 as reported by Jewell and Shepherd (2014).

Measurement	Symbol	Value	Units
Mach number	M	4.55	—
Velocity	U_∞	3051	m/s
Stagnation enthalpy	h_0	7.97	MJ/kg
Static temperature	T_∞	1783	K
Density	ρ_∞	0.104	kg/m^3
Unit Reynolds number	Re_∞	5.99×10^6	1/m

experiment and shot 2723 in T5, one can observe that the other freestream parameters differ significantly between both facilities. This matter will be further discussed later on.

10 Experimental procedure

Before experimentation begins, the MSL is mounted and aligned in the test section. The windows of the test section were removed and the 2" outer diameter pipe was clamped into place (Figure 12). Thermocouple wiring was fed through a tube that was secured at the bottom of the vacuum tank. The wiring was fastened to analog connectors that are shielded from the hypervelocity flow with a protective covering. Once alignment is complete, viewing ports are reinstalled.

Figure 13 shows the various parts of the T5 facility. For the shots done in this experiment, the heavy piston (120 kg) was loaded into the launch capsule. The compression tube is filled with a mixture of Argon and Helium in a process called tailoring to achieve the highest amount of test time. The condition desired used 84% Helium and 16% Argon at a pressure of 109 kPa. The secondary reservoir (2R) is filled with compressed air at high pressures. The shock tube is filled with pure CO_2, to simulate a Martian environment, at a pressure of 71 kPa, and the test section is vacuumed to achieve a low pressure of air.

There is a steel diaphragm in the compression tube-shock tube junction and a mylar diaphragm just downstream of the nozzle throat. When the facility is ready to launch, the 2R high pressure air is let in behind the piston which adiabatically accelerates the piston down the compression tube and pressurizes the gas in front of it. This high pressure breaks the steel diaphragm at approximately 110 MPa and sends a shock with a speed ranging from 2 to 5 km/s down the compression tube. The shock hits the nozzle wall, breaks the mylar diaphragm and reflects back towards towards the compression tube. When both the first shock and reflected shock pass through the gas, it creates a high temperature, high pressure stagnated gas. This gas is then sent through the converging diverging nozzle to create a high enthalpy, high speed flow. The test gas reaches a steady state for approximately 1 ms. For a more detailed explanation on how T5 is run, see Hornung (1992).

In order to prepare for a test, all components of the shock tube, compression tube, and test section are positioned and secured. A checklist containing the standard procedure is used to prepare the entire tunnel for the desired test condition. This involves testing the data acquisition, pressurizing the compression and shock tube at the correct levels, and translating

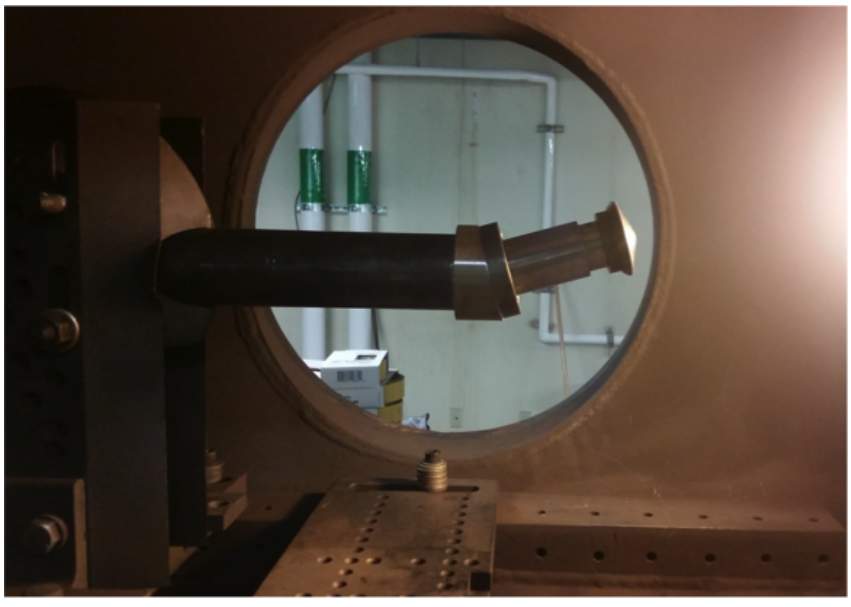

Figure 12: MSL model clamped into test section of T5.

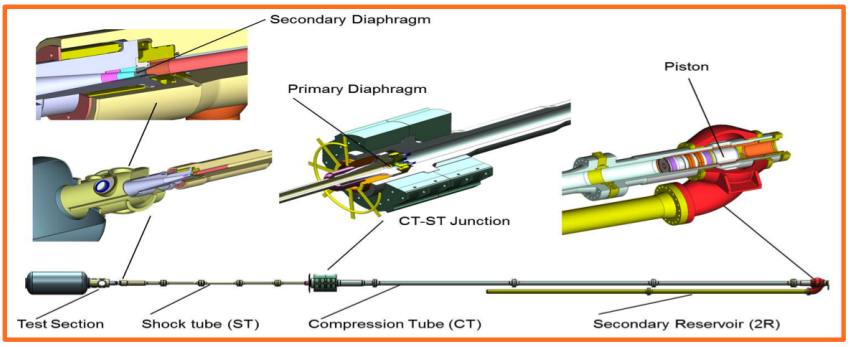

Figure 13: CAD drawing giving an overview on how the T5 shock tunnel facility is run.

the tunnel to account for recoil. For safety, a minimum of two people must be present in the preparation phase. To also minimize risk of danger, the facility also checks the progress of the checklist through a series of switches and sensors. If the user skips a step, the facility will not fire and indicates the missing step with a LED. Once all preparations are complete, a warning siren is activated and seconds later the piston is fired.

After a successful shot, the facility is vented to the outside air and then separated into its three sections. Due to the dissociation of CO_2, free carbon coat the inner walls of the shock tube. In order to obtain a relatively "clean" flow, the facility is thoroughly cleaned. A standard cleaning procedure for T5 is used to remove all impurities in the shock tube. Throughout the history of the facility, it was found that the quality of the cleaning had an impact on where flow transition occurs (Jewell (2014)).

Before an additional test is conducted, the collected data must be analyzed and gaged for its quality. Thermocouple probes often fail after a series of tests. As a result, it is important to find any defective probes before performing another high risk experiment. Software written and used by the laboratory was used to plot all data to easily see any discrepancies. Faulty thermocouples are easily identified by a noisy, unsteady voltage output. It is also valuable to inspect pressure traces at the reservoir location to estimate the effective test time. If pressures are not steady during test time, it may suggest that the driver gas composition may be adjusted for better tailoring. Information like this is valuable when preparing for a second test.

11 Results

In order to study the heat flux at the surface of the MSL heat shield's model, a total of three shots have been performed in the T5 reflected shock tunnel. This section of the report will mainly focus on the first two shots, due to technical issues with the third shot. More details will be given about these technical issues later on.

Post-processing of the data obtained during the first two shots have been performed using a *Matlab* code that was developed over the years by the people working in the T5 research group. Only very minor modifications have been done to this code in order to display the results in a convenient way for the geometry under consideration (this code is available upon request). It is however too large to be included in this report. It is to be noted that this code implements the calculation of the heat flux from the temperature trace recorded by the acquisition system for each one of the thermocouples. Very briefly, the heat transfer rate is deconvolved from the temperature traces by using a Fourier method. This specific methodology is thoroughly explained in the thesis of Sanderson (1995).

Following both main experiments, the freestream conditions have been estimated using a 2D nozzle flow calculation with the *DPLR nozzle code*. The resulting test conditions are shown in Table 3 along with the parameters corresponding to the HET experiment for the sake of comparison. Most parameters shown in this table have already been introduced. It is worth noting that Re_D is the Reynolds number based on the diameter of the model, while Re is a unit Reynolds number, a quantity commonly used to characterize hypersonic flows. Further, X corresponds to the mole fraction of the freestream flow with the subscript indicating the chemical species[4]. Lastly, it is worth noting that the calculated values of U^3 for shots 2829 and 2830 are respectively within 1.3% and 2.3% of the calculated value of U^3 for the experiments conducted in the expansion tube. Said otherwise, the freestream velocity of T5 successfully matches the freestream velocity of the HET, thus giving hope for a reasonable match between the heat fluxes.

11.1 Heat Fluxes

As mentioned earlier, the heat fluxes have been computed for both of the experiments conducted in T5. The resulting dimensional heat fluxes (q_w) are plotted as a function of the normalized distance x/D in Figure 14. To be more specific, x is the distance between the center of the thermocouple and the axis of symmetry of the model, and D is the diameter of the model. Negative values of x/D correspond to the windward side of the model, and positive values correspond to the leeward side.

It is worth pointing out that the data point for shots 2829 and 2830 corresponds to the average heat flux over the useful test time of the experiment (i.e., constant reservoir pressure). This useful test time is approximately 1 ms in the current case. The error bars shown on the plot do not give an indication of the actual error on the heat flux. Instead, the error bars extend 1 standard deviation above and below the average heat flux. As a result, they indicate the amount of fluctuations in the heat flux values over the useful test time. It should be recalled that the approximate error on the heat flux is 8%. Further, the heat fluxes obtained with shots 2829 and 2830 indicate that there is a very good repeatability of the results. Indeed, the variation of the heat fluxes between both experiments is essentially within the experimental error.

For the sake of validation and comparison, other sets of results are plotted in Figure 14.

[4]The freestream conditions given in Table 3 for the T5 facility are for a station located right at the exit of the nozzle. The model is sitting very close to the exit of the nozzle in the test section.

Table 3: Key parameters characterizing the test conditions of T5, along with the key parameters characterizing the test conditions of the HET experiment as described by Sharma et al. (2010).

Parameter	**T5 - Shot 2829**	**T5 - Shot 2830**	**HET**
Δh_0	7.80	8.04	5.97
U_∞ [m/s]	3046	3082	3059
ρ_∞ [kg/m^3]	0.116	0.114	0.014
P_∞ [kPa]	41.8	42.3	2.7
T_∞ [K]	1718	1750	1172
Re_D [–]	2.98×10^5	2.93×10^5	0.51×10^5
Re [1/m]	5.86×10^5	5.77×10^5	1.00×10^5
M [–]	4.28	4.28	5.72
X_{CO2}	0.7763	0.7633	≈ 1
X_{CO}	0.1424	0.1507	≈ 0
X_{O2}	0.0805	0.0850	≈ 0
X_O	0.0009	0.0012	≈ 0

The reader is referred to the original papers/thesis for a detailed review of the experimental work done in these specific studies. A brief comment is provided for each of the data sets used for comparison:

- The results obtained using the HET expansion tube from Sharma et al. (2010). In this study, the exact same model as the one used in the present work has been used.
- The results of a study conducted in T5 in 2006 by Hornung (1992). In this study, the MSL model used was larger than the model used in the current work. Although several freestream conditions have been tested in 2006, only the data set for the case providing a good velocity match with the current tests has been plotted (i.e., shot 2268 with a freestream velocity of 2900 m/s).
- The results of a study conducted at the Calspan-University at Buffalo Research Center (CUBRC) in the LENS-XX expansion tunnel by MacLean et al. (2015). Again, only the results providing a good velocity match with the present work have been plotted, that is runs 4, 19, 20 and 24. The freestream velocity is roughly 3100 m/s for all of these runs.

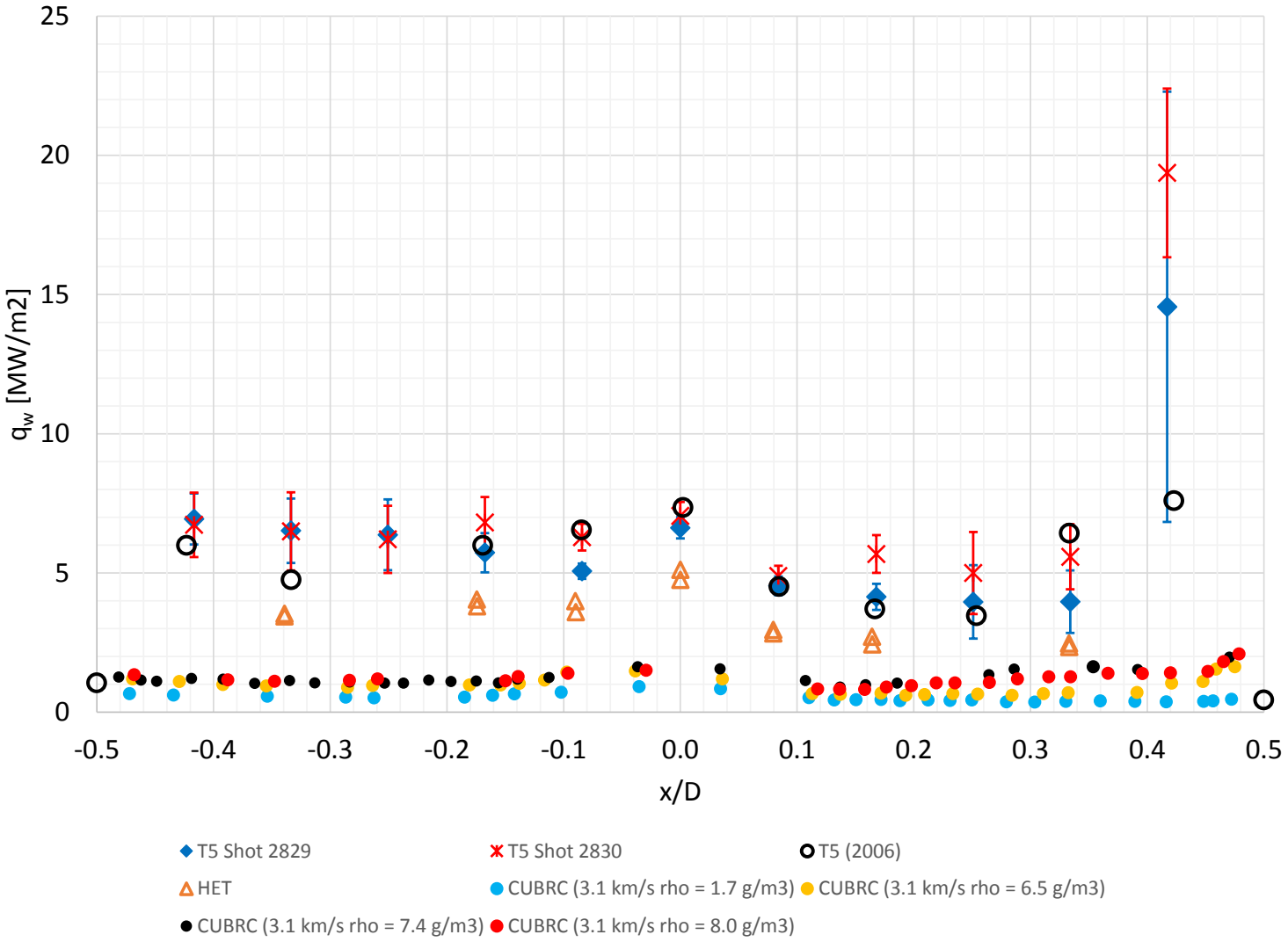

Figure 14: Wall heat flux as a function of the normalized distance from the axis of symmetry of the model. Negative values of x/D correspond to the windward side. Results *T5 (2006)* are obtained from Hornung (1992), *HET* are obtained from Sharma et al. (2010), and *CUBRC* are obtained from MacLean et al. (2015).

Table 4: Comparison of the observed stagnation heat flux with the predicted value obtained with the Sutton-Graves approximation.

	Experimental MW/m^2	Sutton-Graves MW/m^2	Difference %
T5 - shot 2829	6.6	8.7	-24
T5 - shot 2830	7.0	8.9	-21
T5 - 2006 study	5.1	3.1	+65
HET	7.3	3.1	+135

A detailed discussion of the results will be presented in the next few subsections of this document.

11.1.1 Stagnation point heat flux

From the results shown in Figure 14 (T5 shot 2829 and T5 shot 2830), there is a distinctive peak in the wall heat flux close to $x/D = 0$. Such a behavior is as expected, since it is a well known result that the wall heat flux reaches a maximum at the stagnation point. Because the model is at an angle of attack, the stagnation point is not exactly at $x/D = 0$. Instead it will be slightly to the left of it on the plot, i.e. on the windward side, somewhere between x/D of -0.1 and 0. As a result, one can conclude that for both of the tests performed in T5, the stagnation heat flux is slightly above the peaks shown on the plot for $x/D = 0$. The averaged heat fluxes at $x/D = 0$ are respectively 6.6 MW/m^2 and 7.0 MW/m^2 for shots 2829 and 2830.

The approximate values of the stagnation point heat fluxes found above can be compared with the theoretical predictions obtained using the Sutton-Graves equation. According to Braun (2014), this equation takes the following form for a Martian atmosphere:

$$q_w \;=\; 1.9027 \times 10^{-4} \rho_\infty^{0.5}\, V_\infty^3\, R_e^{-1/2} \;. \tag{5}$$

It is to be noted, however, that R_e is the *effective* radius of curvature of the heat shield's blunt nose. As mentioned by Prabhu and Saunders (2012), the ratio of the real nose radius (r) and the overall radius of the model (R) is 0.5 for the MSL heat shield. For this ratio of r/R, Zoby and Sullivan (1966) provide a value of $R/R_e = 0.57$. With this in hand, the effective nose radius of the model can be calculated for the experimental results reported in this document, including those used for comparison purposes (i.e., past T5 results and HET results). The comparison between the observed wall heat flux close to the stagnation point with the value predicted using the Sutton-Graves equation is shown in Table 4.

For the experiments of the present study, the differences between the experimental heat flux and the predicted heat flux are within 25%. Further, the experimental heat flux is *lower* than the predicted one, which is in agreement with the fact that the stagnation point does not exactly lie at $x/D = 0$, thus indicating that the peak lies somewhere between two thermocouples with a slightly higher heat flux than what is shown for $x/D = 0$. In the contrary, there are large unexplained discrepancies between the approximate Sutton-Graves equation and the experimentally measured heat fluxes for the past T5 study and the HET study.

11.1.2 General trend of the wall heat flux

Returning to Figure 14 and focusing on the results of the present study, the wall heat flux is slightly higher on the windward side than it is on the leeward side. This behavior is in qualitative agreement with the results previously published in the literature. This, for example, can be clearly observed in both the experimental results and the numerical predictions of MacLean et al. (2015). Further, the current results show a behavior which is very characteristic of laminar flows, where the wall heat flux essentially monotonically decreases as we move away from the stagnation point. This statement is generally true, except for the edge of the model on the leeward side. Indeed, for both shots, the very last thermocouple on the leeward side indicates a significant increase of the heat flux. The temperature trace given by this specific thermocouple appears to be well behaved, and, therefore, having a faulty thermocouple does not seem very probable. Comparing the present results with those previously published in the literature, the most probable explanation to this increased heat flux would be a laminar to turbulent transition of the flow. Further, the laminar to turbulent transition is expected to first happen on the leeward side based on previous results. This can be seen in the results of Hornung (1992); MacLean et al. (2015) for example. A laminar to turbulent transition would also explain the larger standard deviation for this thermocouple, indicative of larger fluctuations in the instantaneous heat flux.

If one pays careful attention to the results of shot 2830, it appears like the second to last thermocouple on the leeward side also exhibits a slightly increased wall heat flux compared to its neighbor closer to the stagnation point. This, again, would be in agreement with having a laminar to turbulent transition. In order to validate this, a third shot has been performed in T5. Again, the operating conditions have been selected among the repertoire of preexisting test conditions. Further, the expected freestream conditions were such that the Reynolds number would be approximately 2.5 times that of shots 2829 and 2830. The objective was to move the transition point toward the stagnation point. As a result, the turbulent behavior would have been clearly observed on more than one thermocouple. This was expected to provide confirmation that the increased heat flux is indeed attributed to a turbulent flow.

Unfortunately, the pressure sensor in charge of giving the trigger signal to the acquisition system of T5 failed at its task while performing this experiment. As a direct consequence of this, no experimental data was recorded. Due to limited remaining time to conclude this project, and due to another scheduled experiment in T5, it has not been possible to repeat the shot at the time of writing this report. Future work should definitely include a repeat of this experiment.

11.1.3 Comparison with other experimental results

Returning to Figure 14, the dimensional wall heat flux obtained in the present study are in very good agreement with the results from the 2006 study conducted in T5. Not only do the trends agree very well, but the magnitudes of the wall heat flux are also very close. One should note, however, that the Reynolds number of the 2006 experiment was not the same. For this reason, the transition point is not expected to fall on the same location. As a result, it is safer to only compare the heat fluxes exhibiting a laminar type of behavior.

The results obtained in the HET expansion tube using the exact same model as the one used in the present study do not match as well with the results of shots 2829 and 2830 in T5. Although the trends are similar, the wall heat flux is higher in the present experiment. The same can be said about the results obtained using the LENS-XX expansion tube at CUBRC.

One can argue that looking at the dimensional heat flux in order to compare the results ob-

tained using different facilities is not the best way to go. Indeed, considering the non-dimensional wall heat flux seems to be a safer approach. For this reason, Figure 15 shows a similar plot as the one shown in Figure 14, but this time the Stanton number (St) as a function of x/D is shown. The Stanton number is calculated in the following way:

$$St = \frac{q_w}{\rho_\infty U_\infty \Delta h_0} , \tag{6}$$

A very good match is again obtained between the three sets of results obtained using T5. However, the match with the results obtained using both expansion tubes is relatively poor. Even the comparison between the results obtained using HET and LENS-XX, two expansion tubes, is questionable. Furthermore, the results obtained with different test conditions in LENS-XX show some discrepancies. As one can see, the LENS-XX results obtained with a freestream density of 1.7 g/m^3 do not match the other series of data obtained with the same facility. The major differences between this specific set of data and the other sets from CUBRC are certainly the Reynolds number and the density, which are both much lower. Such discrepancies within the results obtained with the same facility suggest the use of a nondimensional heat flux that is corrected for the Reynolds number. One possibility is to use the same formulation as the one used at CUBRC (see MacLean et al. (2015)):

$$St\sqrt{Re_D} = \frac{q_w}{\rho_\infty U_\infty \Delta h_0}\sqrt{\frac{\rho_\infty U_\infty D}{\mu_\infty}} , \tag{7}$$

with μ_∞ being the freestream viscosity (computed using Cantera).

The resulting plot is shown in Figure 16. Again, all results obtained with T5 compare very well when using such a nondimensional heat flux. Further, all the LENS-XX data compare very well together (the discrepancy mentioned earlier is not present anymore). However, there is still an important mismatch between the results obtained using different facilities, i.e., the results of T5 do not match those obtained with HET, which, in turn, do not match the results obtained using LENS-XX. In fact, the nondimensional heat fluxes measured in T5 are roughly 2.5 times lower than those measured in the HET, and roughly 4.5 times lower than those obtained with LENS-XX.

The difficulty of matching the results obtained using different facilities has already been highlighted in a recent review paper by Hollis (2013). In this review, the wall heat flux over an MSL heat shield measured in 5 different hypersonic flow facilities, including T5, have been considered. The authors suggested several reasons to explain the discrepancies. A brief overview is provided here, but the reader is referred to the original paper for more details.

- The results have been obtained in various hypersonic facilities, and the test conditions differ significantly. In fact, there is no real overlap of the test conditions across the five facilities studied.
- Large differences in density will affect the chemical and vibrational processes happening in the flow.
- The operating conditions of the reflected shock tunnels could be influenced by some non-equilibrium vibrational and/or chemical excitation which have not been properly characterized.

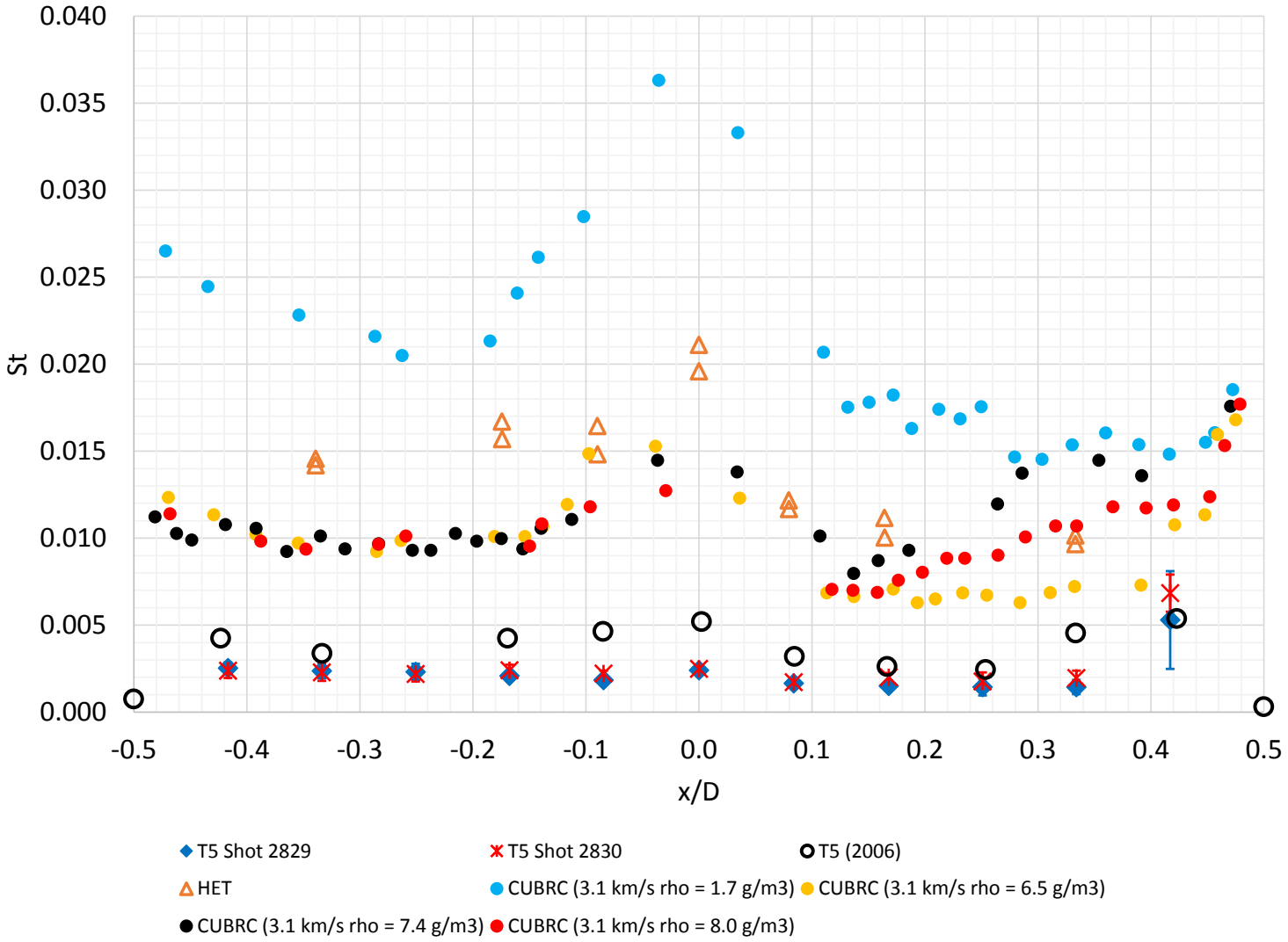

Figure 15: Normalized wall heat flux as a function of the normalized distance from the axis of symmetry of the model. Negative values of x/D correspond to the windward side.Results *T5 (2006)* are obtained from Hornung (1992), *HET* are obtained from Sharma et al. (2010), and *CUBRC* are obtained from MacLean et al. (2015).

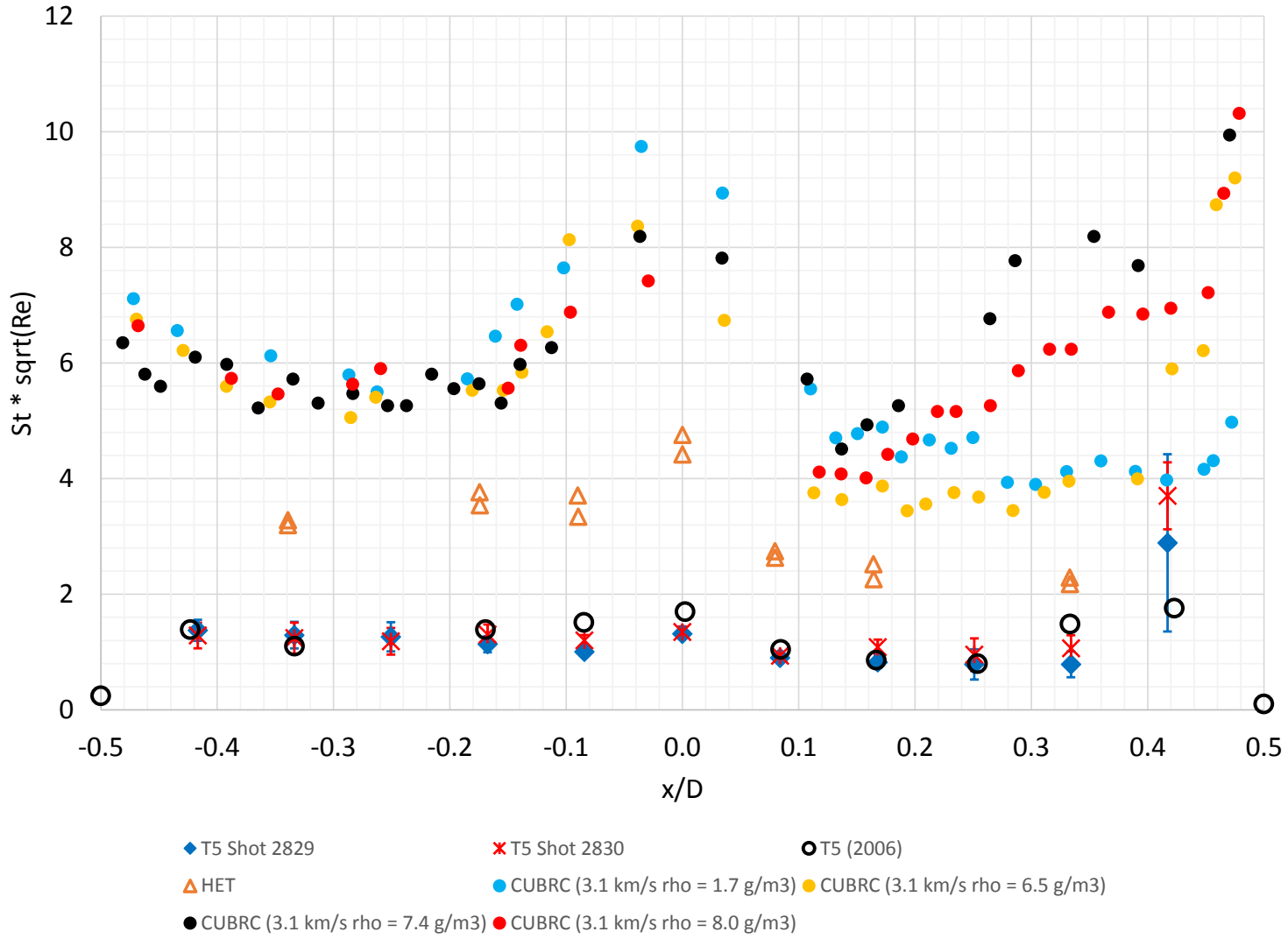

Figure 16: Normalized wall heat flux corrected for the Reynolds number as a function of the normalized distance from the axis of symmetry of the model. Negative values of x/D correspond to the windward side. Results *T5 (2006)* are obtained from Hornung (1992), *HET* are obtained from Sharma et al. (2010), and *CUBRC* are obtained from MacLean et al. (2015).

Another point which is mentioned in the paper is the fact that thermo-physical properties of the material used to build the model could have an influence on the results. However, such an explanation could not explain the differences between the present results and those obtained using the HET since the exact same model has been used.

Obviously, the limited set of results obtained in the present study do not provide enough information to resolve this issue of matching the results coming from different facilities. More research should be conducted on this very interesting issue. However, it is worth pointing out the large differences in the freestream density of the current results with respect to the results used for comparison in this study. The reader may return to Table 3 to find out that the freestream density in T5, with the current nozzle, is approximately one order of magnitude higher than the density in the HET. Further, the freestream density of the HET is roughly 1.75 to 8 times higher than the freestream density of LENS-XX. According to the comments of Hollis (2013) summarized above, this indicates that the chemical and vibrational processes happening in the freestream flow could be significantly different in the various facilities, thus accounting for a part of the discrepancies.

Another difference which is worth mentioning is the fact that the freestream flow of the expansion tube is essentially composed of 100% of CO_2. Indeed, there is not much dissociation happening in such facilities. In the contrary, the freestream flow of T5, for the present work, had approximately 75% of CO_2. This, again, could explain the differences between the results obtained using shock tunnels and expansion tubes. However, this is not of any help for explaining the differences between the results from HET and LENS-XX.

Obviously, finding a way of matching the results obtained with different facilities or, at least, to explain the discrepancies, remains an open question. There could perhaps be a better way of nondimensionalizing the heat fluxes which could provide a better collapse of the data. Indeed, one could question the idea of simply using a Stanton number corrected for the Reynolds number. Maybe some more parameters are required in order to account for the different composition of the gas, and for the different chemical and vibrational processes of the flow.

11.2 Shock standoff distance

As previously mentioned, images of the flow chemiluminescence have been obtained for both shots done in T5. As the amount of light emitted by the flow is very large, the use of a filter to cut a fraction of the light is required. This is needed to avoid saturating the camera. Figure 17 shows the chemiluminescence of the flow for shot 2829. Unfortunately, the filter used did not cut enough light, such that the camera was saturated, and it is not possible to clearly distinguish the main features of the flow ahead of the model. However, with this image it is possible to see that there is an interaction between the supersonic flow and the locking nut on the windward side. Such an observation suggests that a locking disk with the same diameter as the main sting (i.e., 2 inches) should preferably be used if the experiment is repeated in the future. This would help avoiding any feedback effect.

Figure 18 shows the chemiluminescence of the flow for shot 2830. The filter used for this shot cut more of the light, and there is clearly a better resolution of the flow ahead of the model. In fact, one can assume that the beginning of the white region ahead of the model approximately corresponds to the location of the bow shock.

It is also possible to compare the location of the bow shock with the results obtained in the HET. Such a comparison is very easy due to the fact that the same model was used in both experiment. Indeed, a simple overlay of both images provides a qualitative comparison. This is shown in Figure 19. The main conclusion of such a comparison is that the shock standoff

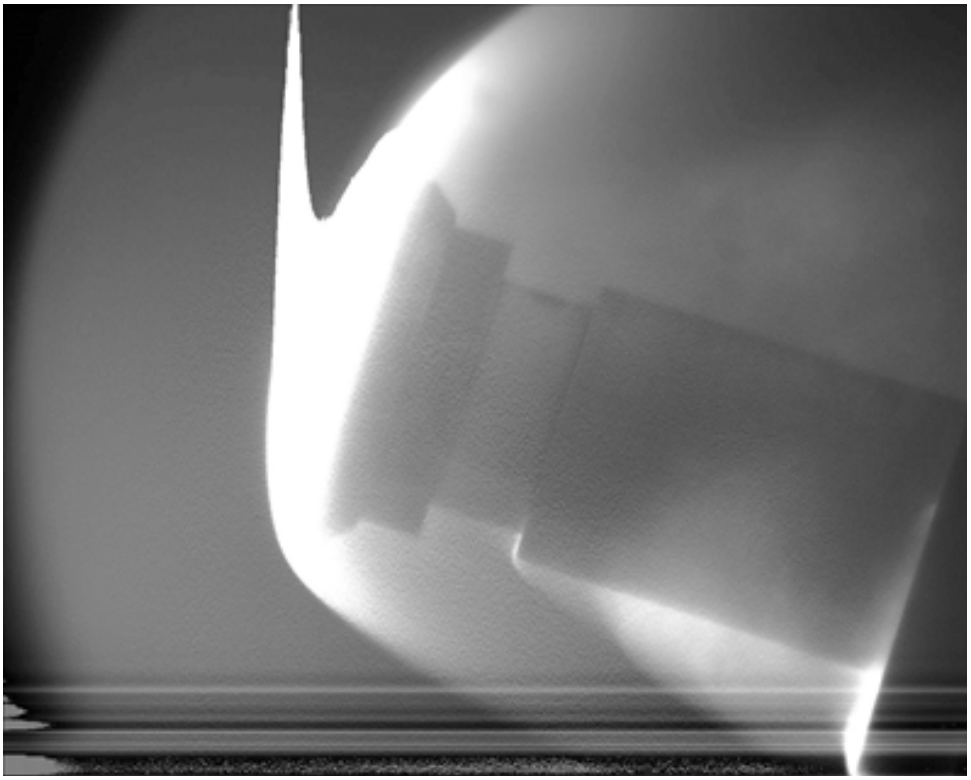

Figure 17: Image of the chemiluminescence of the flow during shot 2829.

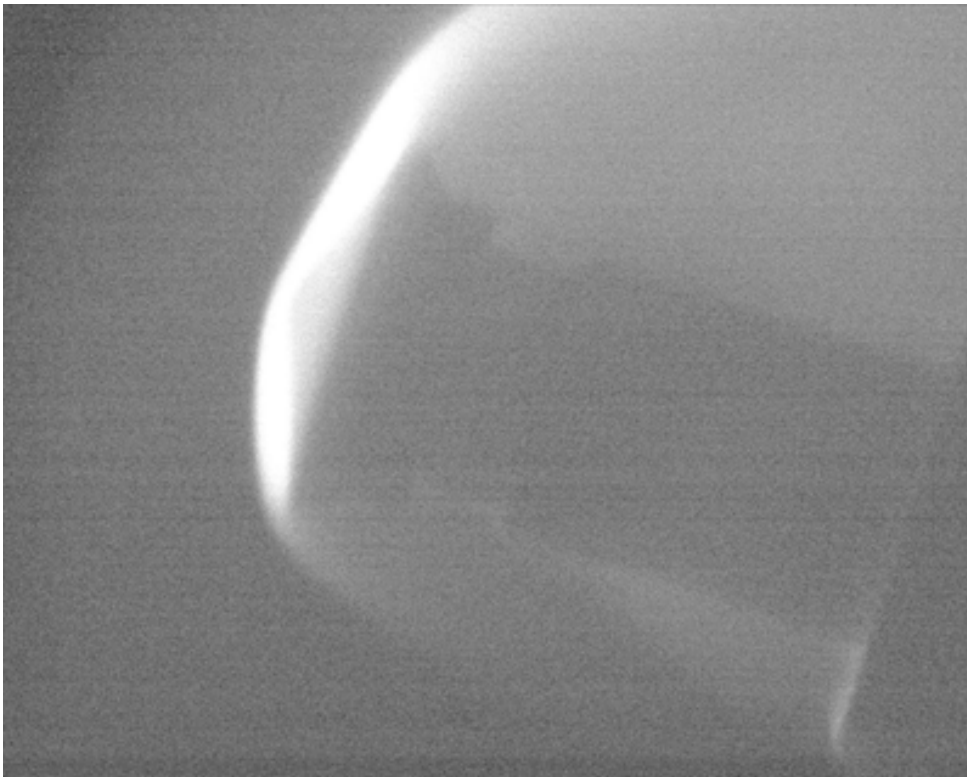

Figure 18: Image of the chemiluminescence of the flow during shot 2830.

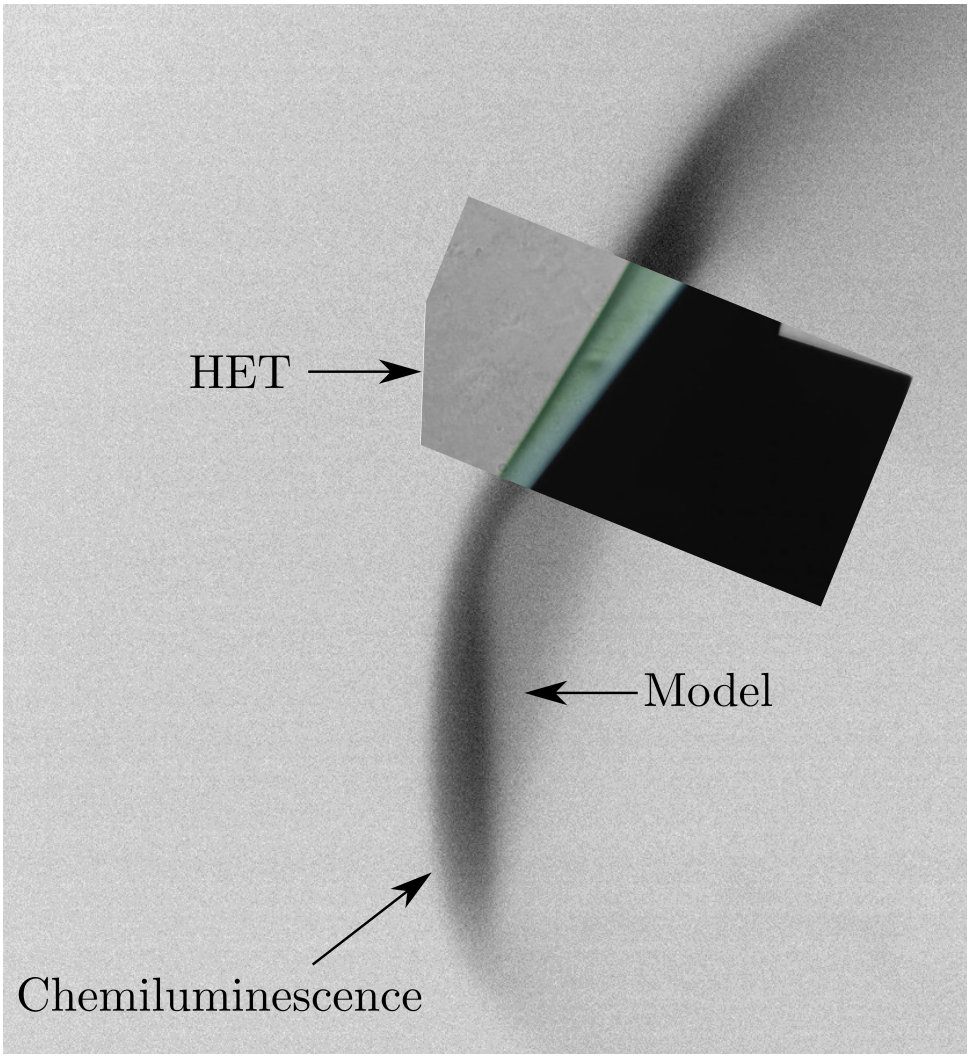

Figure 19: Shock shape comparison between T5 (shot 2830) and the HET. The colors of the image showing the chemiluminescence of the flow have been inverted in order to show more clearly the shape of the shock. The HET data has been obtained from Sharma et al. (2010).

distance of the present experiment is slightly larger than it was for the HET experiment.

Using *Inkscape*, it was also possible to extract an approximate, normalized shock standoff distance for both the T5 experiment (shot 2830) and the HET experiment. In the case of the T5 experiment, the shock is approximately 0.051 diameter ahead of the model's blunt nose. For the HET experiment, the shock is 0.045 diameter ahead of the model's blunt nose. These numbers confirm the qualitative observation previously done using the overlay: the shock standoff distance of the T5 experiment is slightly larger than the one obtained with HET.

It is possible to use very simple ideas to gain physical insights, and find out if this behavior corresponds to what should be expected. One should keep in mind that the methodology used here only provides rough estimates of the shock standoff distance since all assumptions made could be categorized as being first order.

Using Cantera with the Shock Detonation Toolbox developed by Prof. Shepherd's group at Caltech, it is possible to estimate the post-shock conditions of the flow. In fact, it is possible to get the post-shock conditions for both a chemically frozen flow, which gives a good estimate of the conditions just behind the shock, and also at chemical equilibrium, which provides an

Table 5: Estimated post-shock conditions for the T5 experiment (shot 2830) and the HET experiment. The calculations yielding these results have been obtained using Cantera with the Shock and Detonation Toolbox of Prof. Shepherd's group at Caltech.

Parameter	T5 (shot 2830)	HET
T_{fr} [K]	5088	4494
P_{fr} [Pa]	1.08×10^6	0.11×10^6
ρ_{fr} [kg/m^3]	1.08	0.12
T_{eq} [K]	3346	2871
P_{eq} [Pa]	1.11×10^6	0.11×10^6
ρ_{eq} [kg/m^3]	1.41	0.17

estimate of the conditions at some distance behind the shock.

Once the freestream, frozen and equilibrum densities are known, it is possible to use the model of Wen and Hornung (1995) to get an estimate of the shock standoff distance for a point at the surface of the model where the density is equal to the equilibrium density. One should note that this simple model was developed for a sphere, not an MSL model. This is without real consequence as the main purpose of this calculation is only to find out which standoff distance should be larger.

The post-shock conditions of the flow computed with Cantera are shown in Table 5. Note that the subscript *fr* corresponds to the chemically frozen calculation, while the subscript *eq* corresponds to the conditions at chemical equilibrium. Following this, it is possible to estimate the normalized shock standoff distance as:

$$\frac{\Delta}{d} = \frac{0.82}{1+(\rho_{eq}/\rho_{fr})}\frac{\rho_\infty}{\rho_{fr}} , \tag{8}$$

where Δ is the shock standoff distance and d is the diameter of the model. This yields $\Delta/d = 0.038$ for the T5 experiment, and $\Delta/d = 0.0396$ for the HET experiment. The results therefore suggest that there should not be a significant difference in the standoff distance between the T5 and HET experiments (i.e., difference of approximately 4%), and the shock standoff distance in HET should be the slightly larger one. However, the experimental observations suggest the opposite, which is that the shock standoff distance in T5 is approximately 14% larger than in HET. Obviously, this shows that there is yet another discrepancy between the results obtained using different hypersonic facilities. Such discrepancy on the shock standoff distance has also been highlighted in the paper of Hollis (2013) previously mentioned. However, more experimental work is needed in order to hypothesize on the possible causes of such discrepancies.

12 Partial conclusion

Within this part of the report, the process of designing a suitable support for the MSL heat shield previously used in HET has been described. As previously highlighted, the larger aerodynamic forces to be experienced by the model in the test section of T5 required the design of a new sing to avoid failure. Once the design was complete, the sting was promptly manufactured and the experimental phase could begin.

This experimental phase accoomplished three shots in the T5 reflected shock tunnel. The first two shots had the same operating conditions in order to asses the repeatability of the results. For the last shot, a higher Reynolds number was aimed for as a way to investigate the laminar to turbulent transition on the leeward side of the model. However, due to a faulty pressure probe, no data was acquired during this shot.

Despite this technical issue, the first two shots successfully measured the heat flux at the surface of the model. Comparison between the two data sets and comparison with results available in the literature, especially with a previous study conducted using T5, strongly suggested that the results obtained are physically valid. A good quantitative match of the dimensional and non-dimensional heat fluxes has not been obtained with the results obtained using LENS-XX and HET, two expansion tubes.

Although this short project did not aim at resolving the issue of matching the heat fluxes obtained using different facilities, it did confirm that there are indeed some discrepancies. Further work will be needed in order to find a way to collapse all the data obtained with different facilities on a single curve. A better understanding of the physical processes may suggest a better way of nondimensionalizing the heat fluxes. Also, a better standardization of the experiments conducted in different facilities will surely help at solving this open question. Last but not least, future facilities should be designed such that there is a better overlap in the freestream conditions. As of today, the overlap of the freestream conditions is poor. A direct consequence of this is certainly that several parameters must be changed when trying to repeat an experiment conducted in another facility. When so many parameters are varied, it makes it hard to investigate the impact of each. The ideal situation would be to have complete similitude between two facilities, but this is somewhat unrealistic. Instead, simply having a better match of the key parameters would make it easier to understand the physics.

13 Conclusion and future work

Following this research project, more experimental work should be achieved. First, the double cone should be instrumented and mounted in the test section of T5. Several shots should be performed covering a wide range of operating conditions. This will allow to add a substantial amount of data to the worldwide database. Such a contribution will be significant to the development of CFD. The match between those results and those obtained with other facilities should also be investigated.

The MSL heat shield should also be further investigated in T5. Again, this will add some more data to the worldwide database, thus helping the CFD community to develop accurate models. These models will play a crucial role in future extraterrestrial exploration. Since GALCIT will soon be home of both HET and T5, this will facilitate the investigation of the heat flux mismatch between two hypersonic facilities. Indeed, it will be relatively easy to conduct the same experiment in both HET and T5, thus providing useful data for investigation this matter. Such an investigation will prove useful in the long run.

As a final comment, and also on a more personal perspective, the authors of this document have had the chance to develop very important skills that are paramount to successful graduate research. These skills include:

- Being able to perform a thorough survey of the literature.
- Being able to design some of the components needed for the experimental setup.
- Being able to select relevant experimental conditions serving adequately the purpose of the study.
- Being able to conduct an experiment in a safe and accurate manner.
- Being able to asses the validity of the experimental results.
- Being able to draw physically sound conclusions from the data obtained.

Bibliography

Adler, Wright M. Campbell C. Clark I. Engelund W. Rivellini T., M. Entry, descent, and landing roadmap technology area 09. Technical report, NASA, 2010. *Page 13*

Anderson, J. AIAA Education. AIAA, Reston, Virginia, United States, 2006. *Page 18*

Braun, R. Planetary entry, descent and landing. Technical report, Georgia Institute of Technology, 2014. *Pages 14, 18, and 25*

Edquist, Dyakonov A. A. Wright M.J., K.T. and C.Y., Tang. Aerothermodynamic environments definition for the mars science laboratory entry capsule. *AIAA*, 2007-1206, 2007. *Page 13*

Engineering Toolbox. Sae grade 8 steel bolts. URL `http://www.engineeringtoolbox.com/steel-bolts-sae-grades-d_1426.html`. Accessed: 2014/05/30. *Page 15*

Holden, Wadhams T.P. Harvey J.K., M.S. and Candler, G.V. Comparisons between measurements in regions of laminar shock wave boundary layer interaction in hypersonic flows with navier-stokes and dsmc solutions. *NATO-OTAN*. *Page 3*

Hollis, Prabhu D., B. Assessment of laminar, convective aeroheating prediction uncertainties for mars entry vehicles. *Journal of Spacecraft and Rockets*, 50(1):56–58, 2013. *Pages 13, 27, 30, and 33*

Hornung, H. Performance data of the new free-piston shock tunnel at galcit. Technical report, California Institute of Technology, 1992. *Pages 20, 23, 24, 26, 28, and 29*

Jewell, J. S. and Shepherd, J. E. T5 conditions report, shots 2526-2823. Technical report, Graduate Aerospace Laboratories, California Institute of Technology, June 2014. *Pages 14, 18, and 19*

Jewell, J.S. *Boundary-layer transition on a slender cone in hypervelocity flow with real gas effects*. PhD thesis, California Institute of Technology, 2014. *Page 21*

MacLean, M., Dufrene, A., Carr, Z., Parker, R., and Holden, M. Measurements and analysis of mars entry, descent, and landing aerothermodynamics at flight-duplicated enthalpies in lens-xx expansion tunnel. In *53rd AIAA Aerospace Sciences Meeting*, Kissimmee, Florida, 2015. *Pages 14, 23, 24, 26, 27, 28, and 29*

Nompelis, Candler G.V., I. Numerical investigation of double-cone flow experiments with high-enthalpy effects. *AIAA*, 2010-1283, 2010. *Pages 3, 4, 5, and 11*

Prabhu, D. K. and Saunders, D. A. On heatshield shapes for mars entry capsules. In *50th AIAA Aerospace Sciences Meeting*, Nashville, Tennessee, 2012. *Page 25*

Sanderson, S. R. *Shock wave interaction in hypervelocity flow*. PhD thesis, California Institute of Technology, 1995. *Page 22*

Sharma, M., Swantek, A. B., Flaherty, W., Austin, J. M., Doraiswamy, S., and Candler, G. V. Experimental and numerical investigation of hypervelocity carbon dioxide flow over blunt bodies. *Journal of Thermophysics and Heat Transfer*, 24(4), 2010. *Pages 18, 19, 23, 24, 28, 29, and 32*

Swantek, Andrew. *The Role of Aerothermochemistry in Double Cone and Double Wedge Flows*. PhD thesis, University of Illinois, Urbana-Champaign, 2012. *Pages 3, 4, 5, and 6*

Swantek A.B., Austin J.M. Heat transfer on a double wedge geometry in hypervelocity air and nitrogen flows. In *50th AIAA Aerospace Sciences Meeting*, Nashville, Tennessee, 2012. *Pages 3, 5, and 11*

Wen, C. Y. and Hornung, H. G. Non-equilibrium dissociating flow over spheres. *Journal of Fluid Mechanics*, 299, 1995. *Page 33*

Zoby, E. and Sullivan, E. Effect of corner radius on stagnation point velocity gradients on blunt axisymmetric bodies. *Journal of Spacecraft and Rockets*, 3(10), 1966. *Page 25*

Appendix A Machine drawings for double cone and sting

This section contains the drawings sent to the machine shop for fabrication of the parts for the double cone by the GALCIT machine shop. A total of 39 machine hours went into the double cone, flange, and sting. Note the flange was welded onto the sting by Bahram Valiferdowsi.

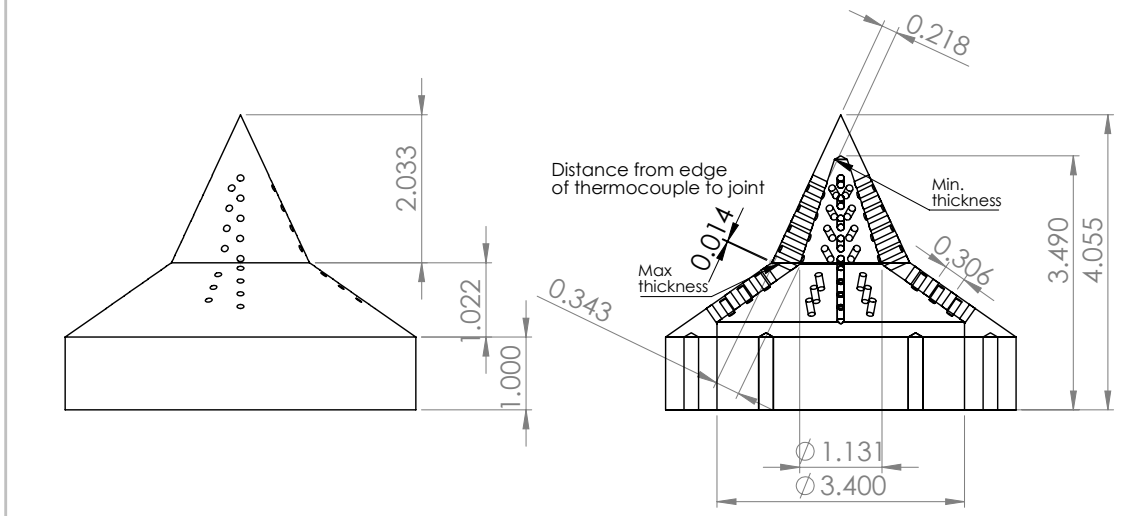

Ratio of diameters is now 4.815/1.896=2.53956
Compared to Nompelis = 2.54
Swantek=2.5406

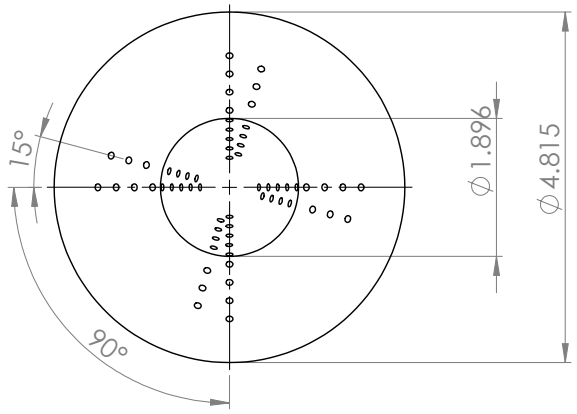

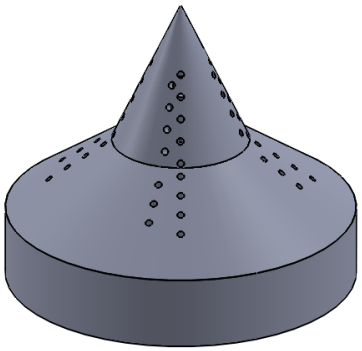

4 symmetric sets of thermocouples

UNLESS OTHERWISE SPECIFIED: DIMENSIONS ARE IN INCHES SURFACE FINISH: TOLERANCES: LINEAR: ANGULAR:		FINISH:		DEBUR AND BREAK SHARP EDGES	DO NOT SCALE DRAWING	REVISION
	NAME	SIGNATURE	DATE		TITLE: DOUBLE CONE	
DRAWN						
CHK'D						
APPV'D						
MFG						
Q.A				MATERIAL: A2 TOOL STEEL	DWG NO. MGL, JCV, NJY	A4
				WEIGHT:	SCALE:1:5	SHEET 1 OF 1

Figure 20: Double Cone machine drawing.

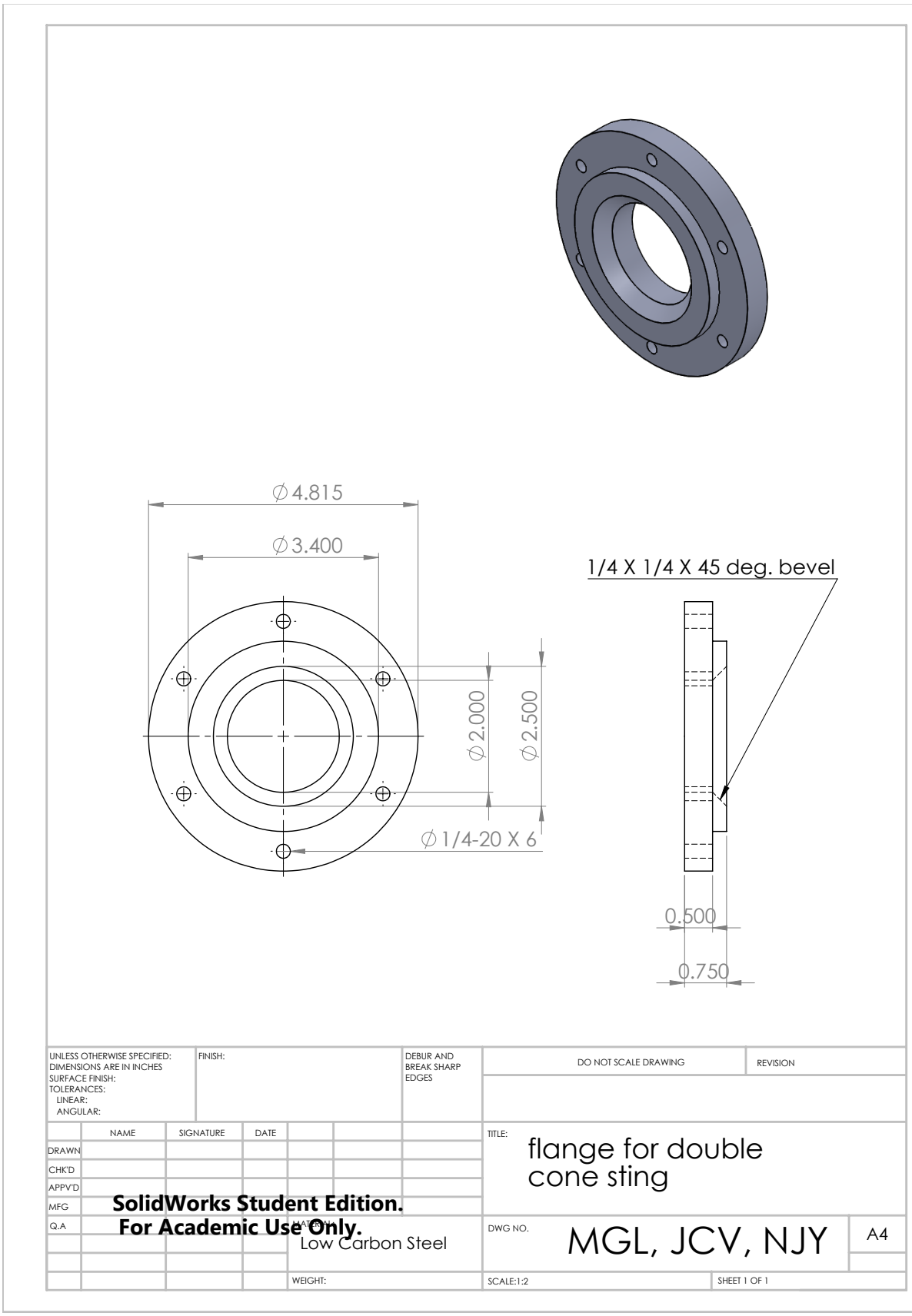

Figure 21: Flange machine drawing.

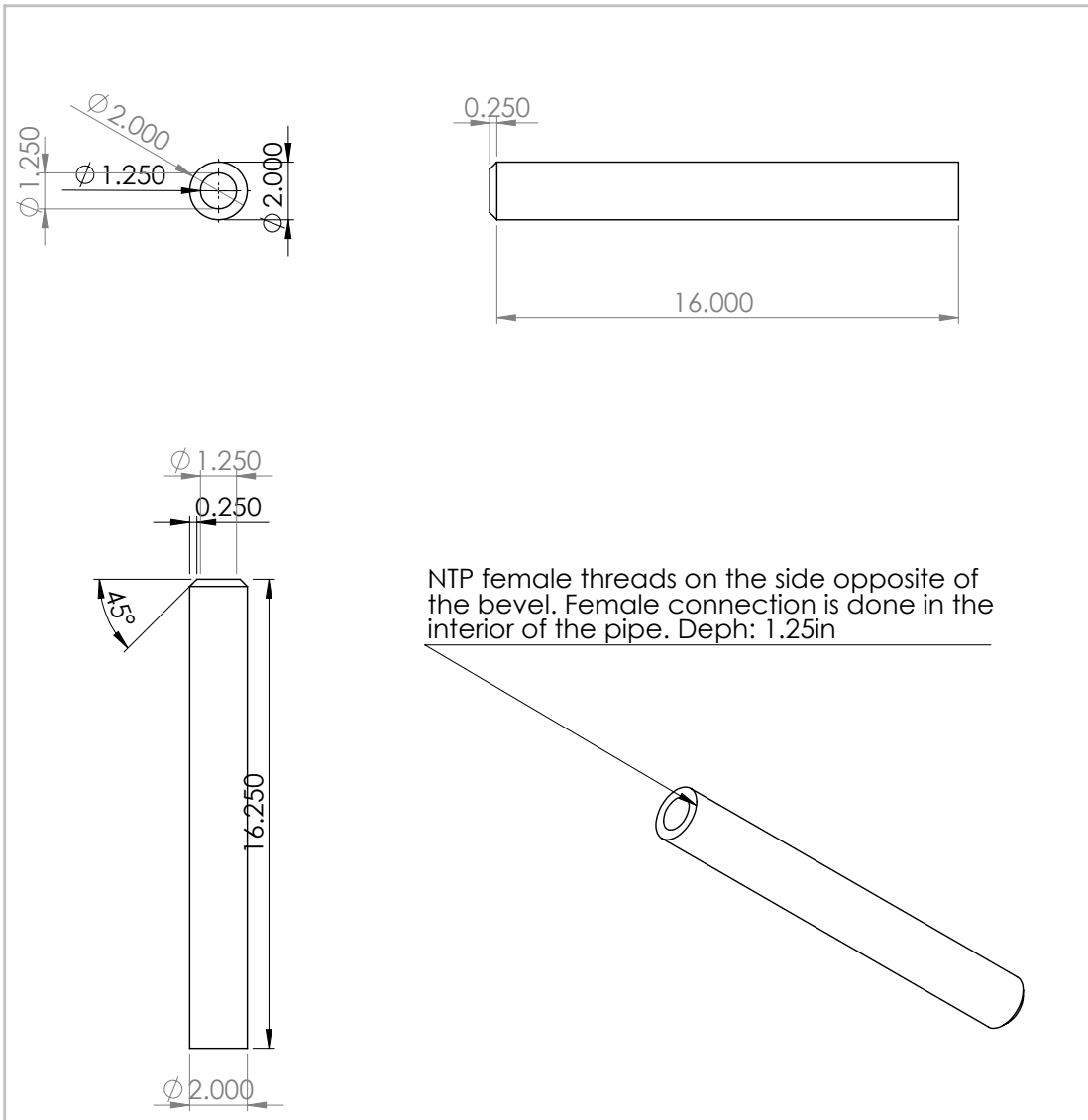

Figure 22: Sting pipe machine drawing.

Appendix B Machine drawings for MSL model and sting

This section contains the drawings sent to the machine shop for fabrication of the parts for the MSL model sting redesign by the GALCIT machine shop. A total of 22.5 machine hours went into the various parts.

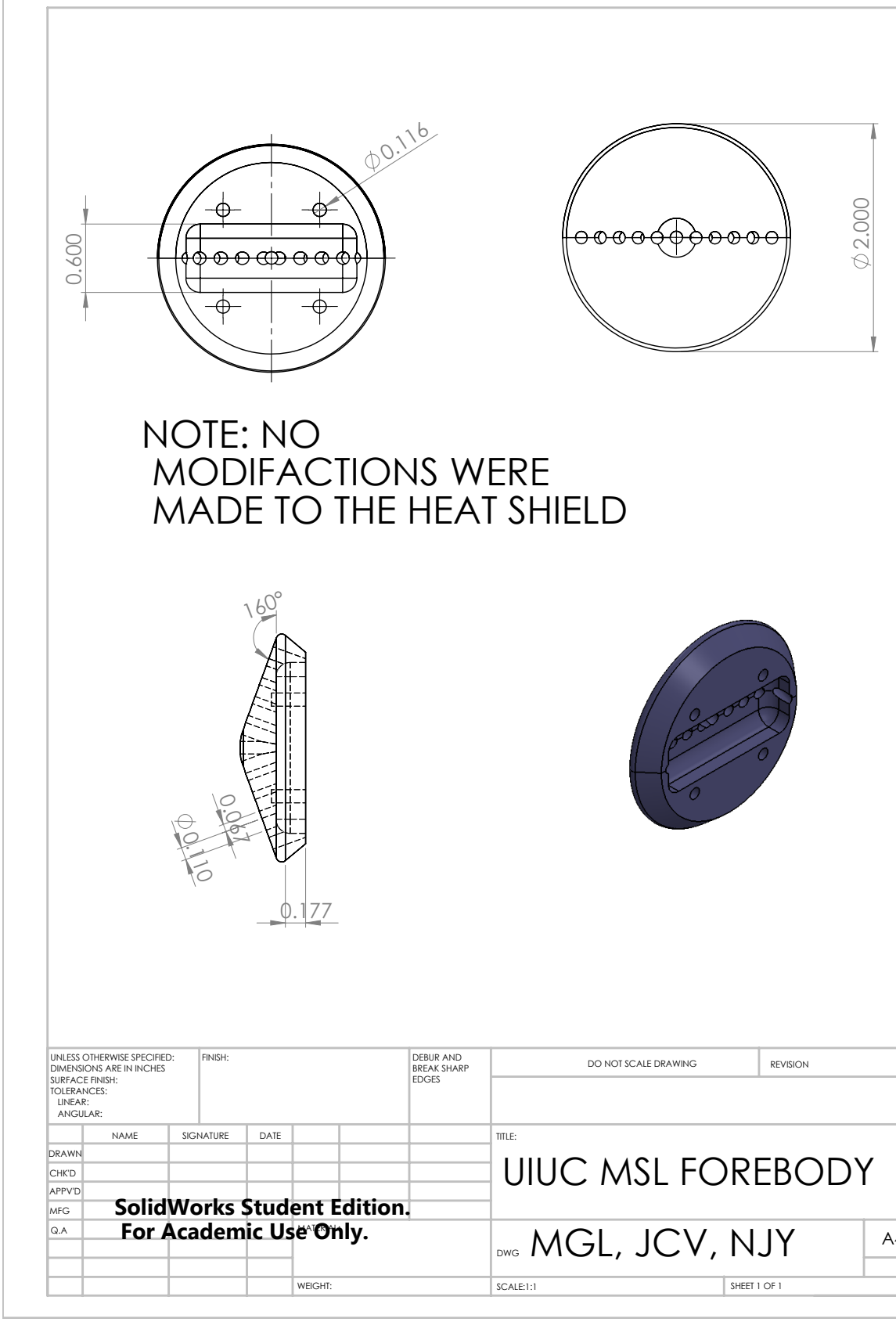

Figure 23: MSL forebody machine drawing.

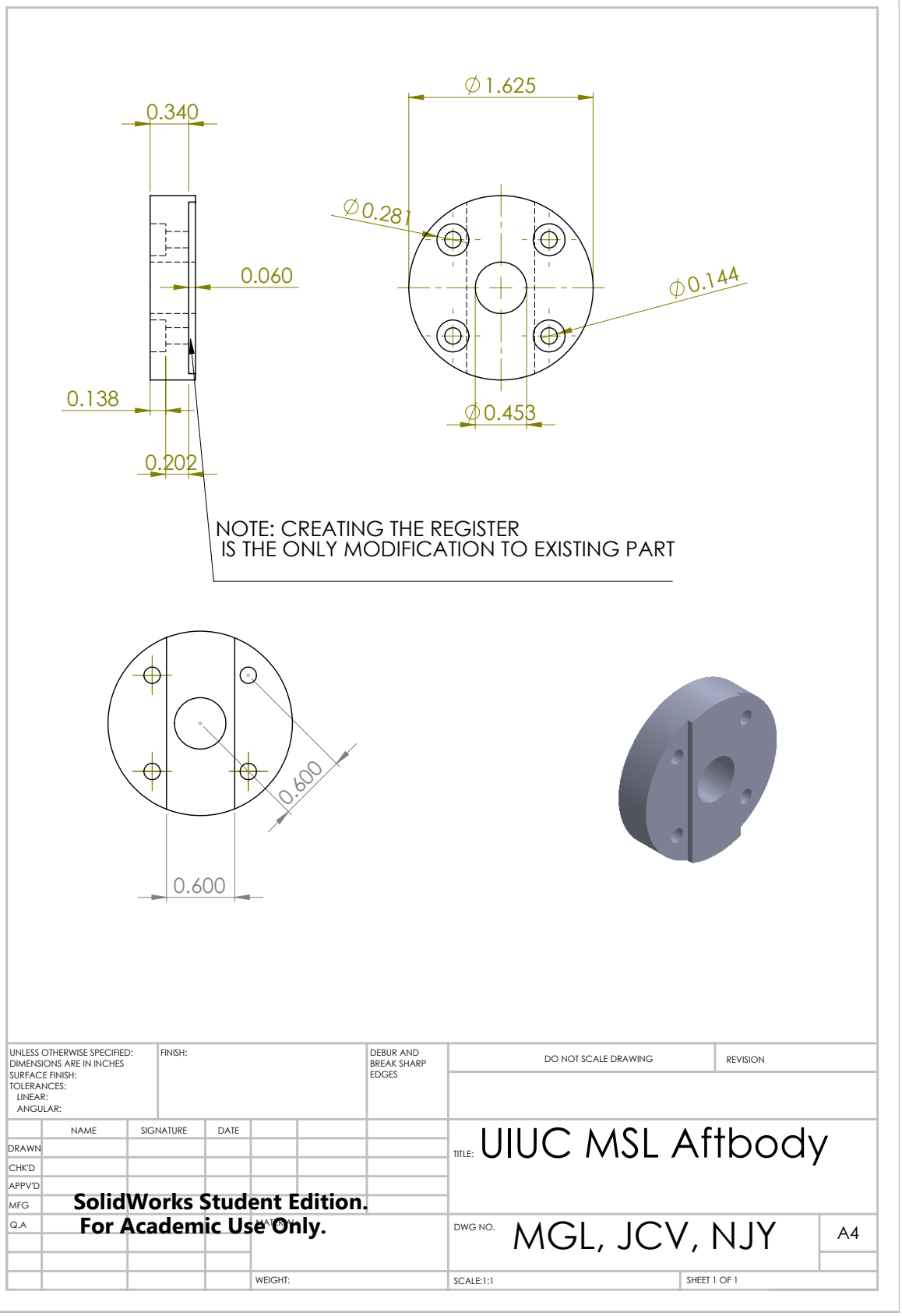

Figure 24: MSL aftbody drawing.

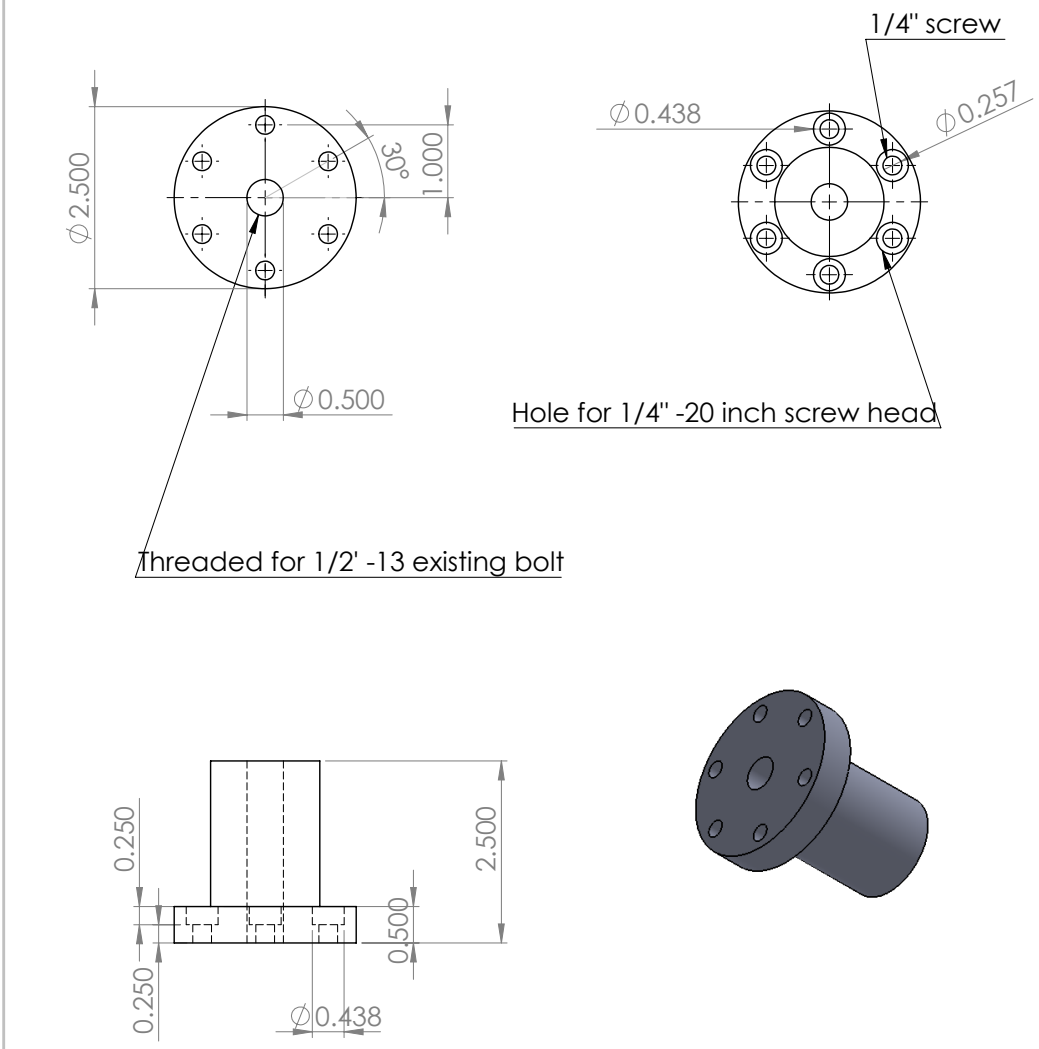

UNLESS OTHERWISE SPECIFIED: DIMENSIONS ARE IN INCHES SURFACE FINISH: TOLERANCES: LINEAR: ANGULAR:		FINISH:		DEBUR AND BREAK SHARP EDGES	DO NOT SCALE DRAWING		REVISION
	NAME	SIGNATURE	DATE		TITLE: MSL Strut		
DRAWN							
CHK'D							
APPV'D							
MFG							
Q.A					DWG NO. MGL, JCV, NJY		A4
				WEIGHT:	SCALE:1:2	SHEET 1 OF 1	

Figure 25: MSL strut machine drawing.

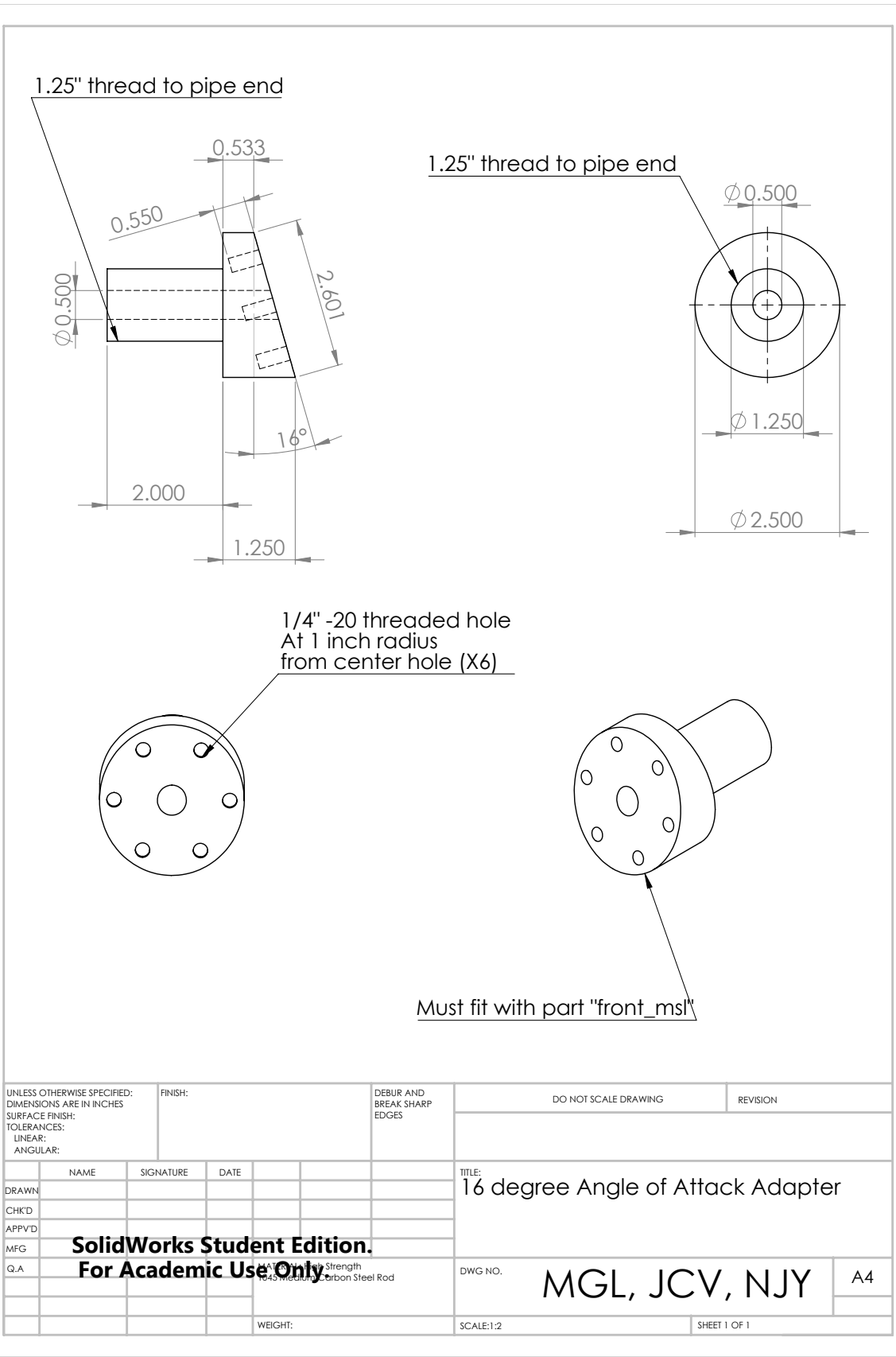

Figure 26: MSL 16° incline mount machine drawing.

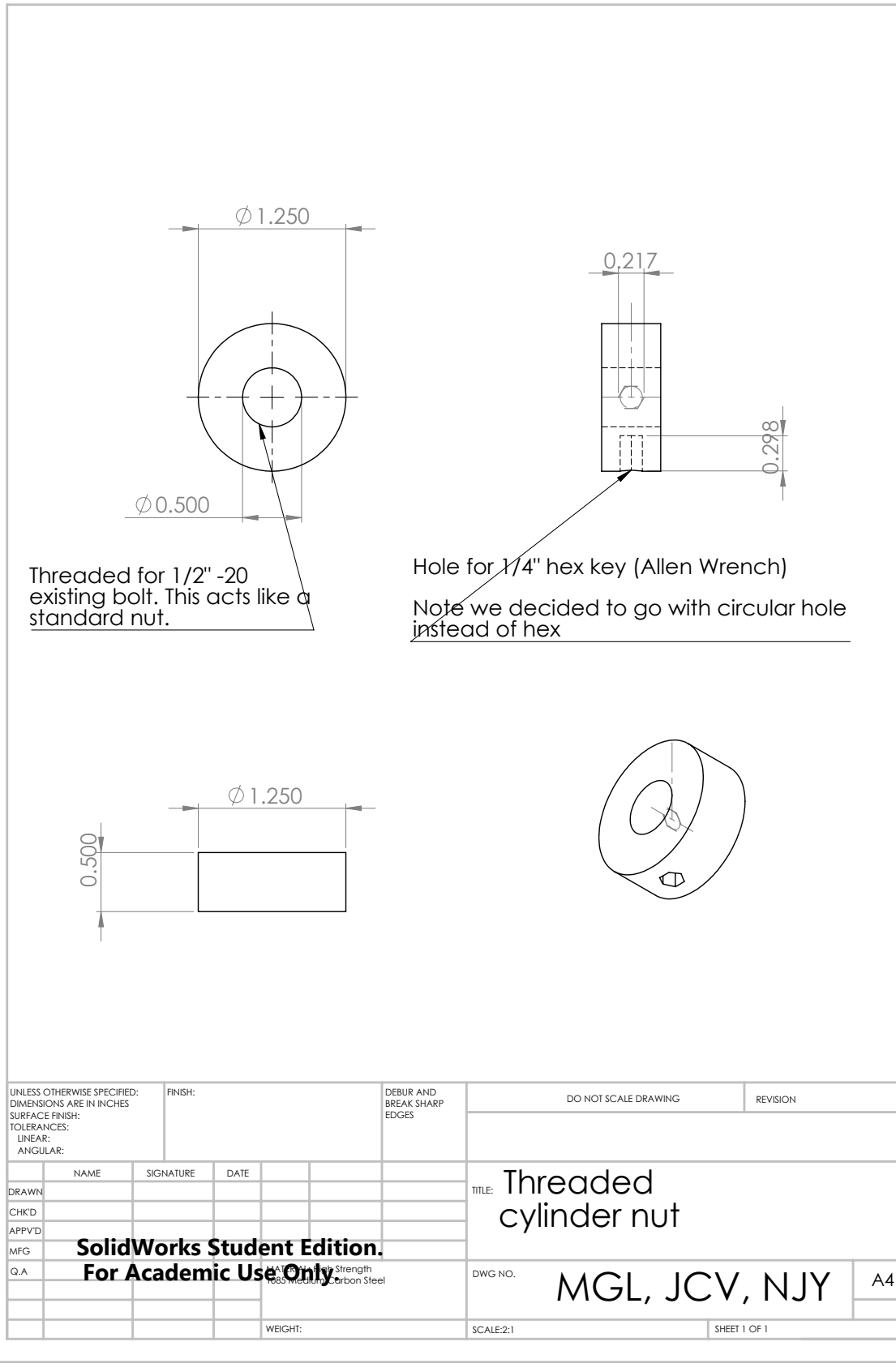

Figure 27: threaded cylinder nut machine drawing.

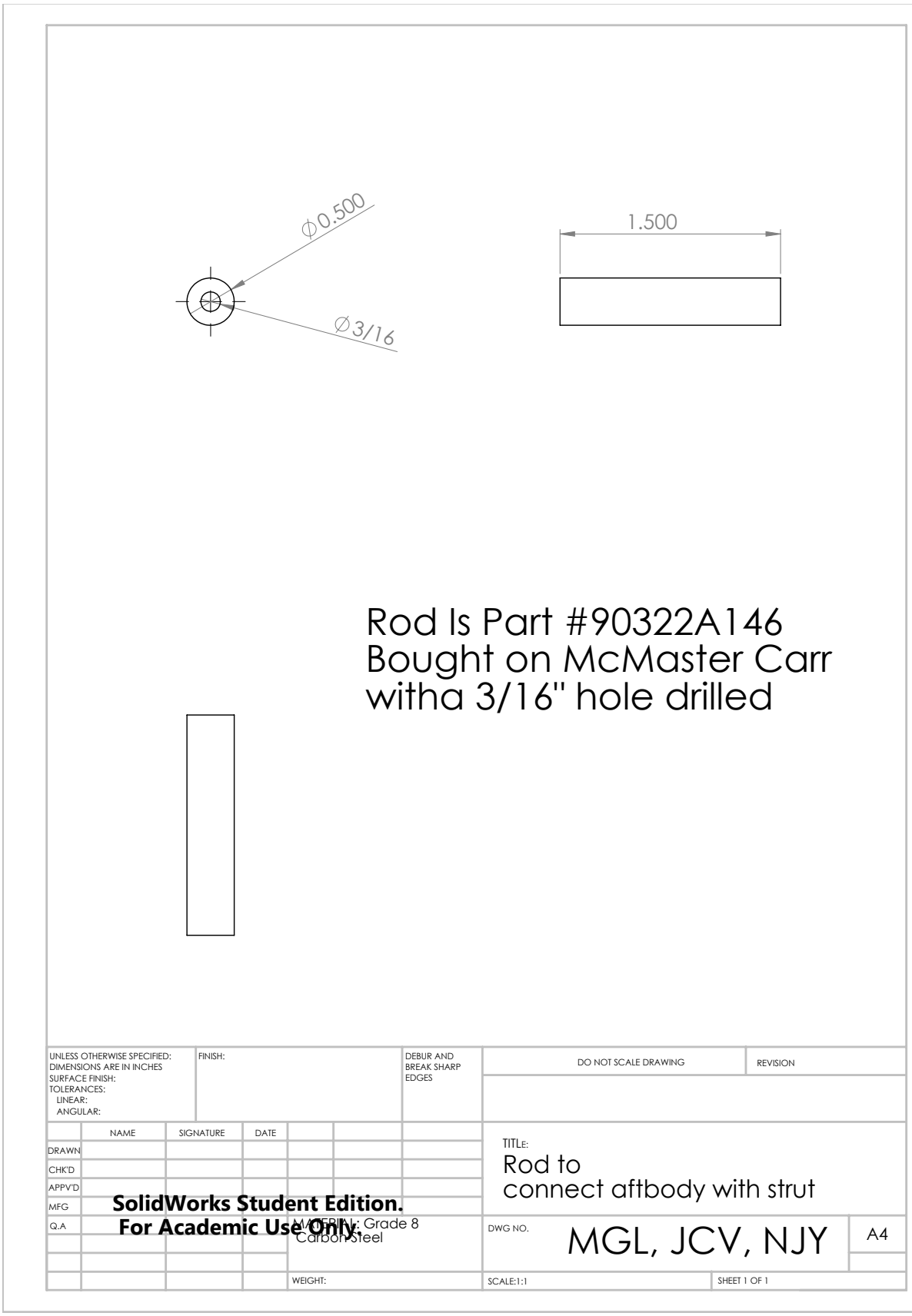

Figure 28: Connecting rod machine drawing.

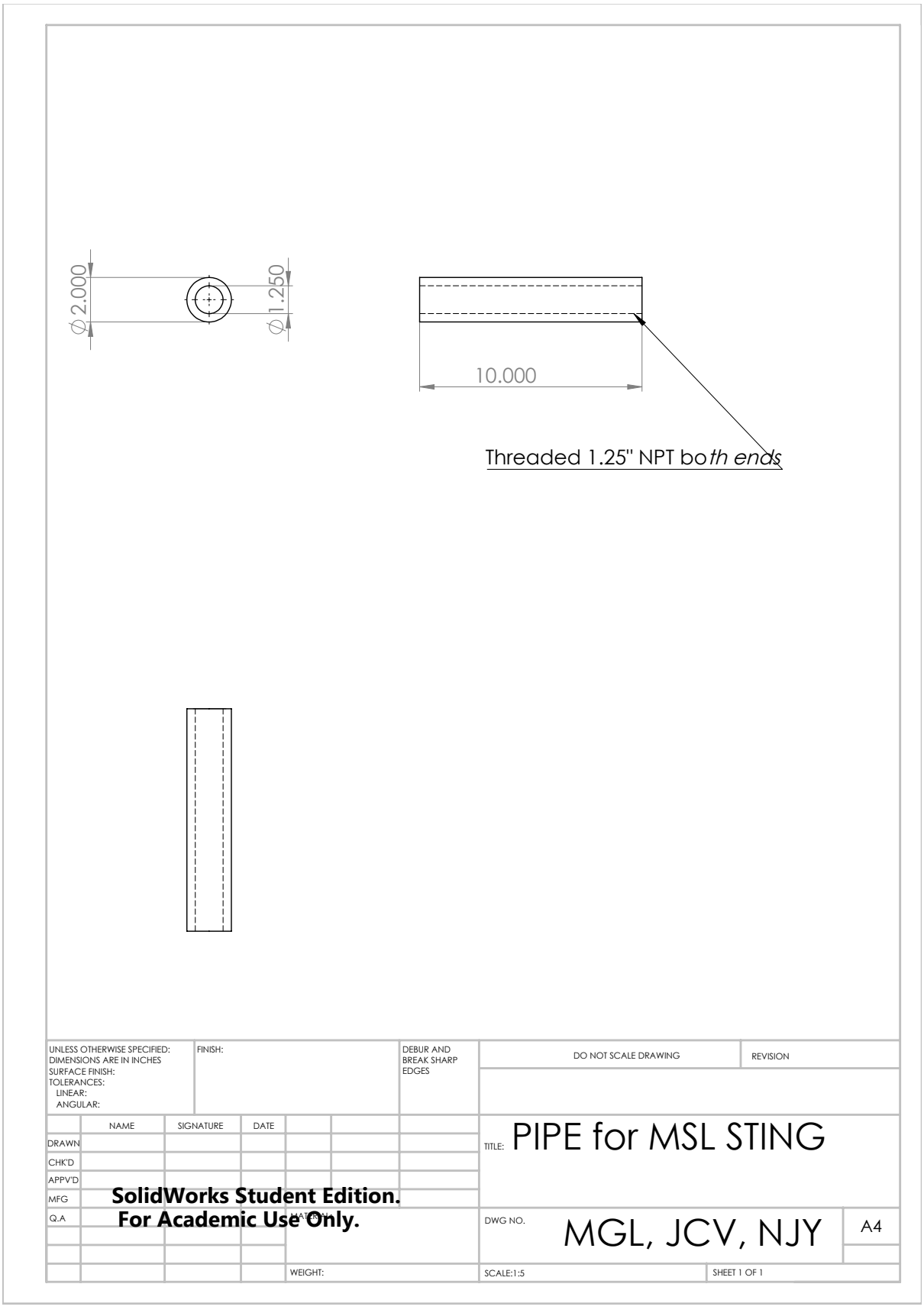

Figure 29: Sting pipe machine drawing.

Appendix C Expense sheet

This section contains the expenses during the AE104C term. The expense sheet does not include the cost of running the T5 facility and the many man hours devoted to this project.

EXPENSE SHEET

McMaster-Carr

Order on 04/01						
Line	**Product #**	**Product**	**Ordered**	**Price**	**Total**	**Note**
1	8443K28	Wear-Resistant A2 Tool Steel, Oversized Rod, 6" Diameter, 6" Long	1	260.1	260.10	Made into double cone model and flange face
2	1388K411	Low-Carbon Steel Sheet, 3/4" Thick, 6" X 6", Ground Finish	1	57.79	57.79	Unused (originally for flange face)
3	7767T81	Low-Carbon Steel Tubing, 2" OD, 1.250" ID, .375" Wall Thickness, 3' L	1	99.04	99.04	For double cone sting
4	90342A130	Alloy Steel Socket Head Cap Screw with Lock Washer, 1/4"-20 Thread, 1-1/4" Length, packs of 1	8	2.4	19.20	Sting to double cone connection
				Sum:	**436.13**	

Order on 04/07						
Line	**Product #**	**Product**	**Ordered**	**Price/Each**	**Total**	**Note**
1	5350K48	Zinc-Plated Steel Barbed Hose Fitting, High Flow Barbed X Male for 3/4" Hose ID, 1" Pipe	1	6.06	6.06	Double Cone: Plumbing sting to hose connector
2	4464K539	Type 304 Stainless Steel Threaded Pipe Fitting, 1-1/4 X 1 Pipe Size, Reducing Coupling, 150 PSI	1	14.96	14.96	Double Cone: Female to female reducer from 1.25" to 1" for sting to hose fitting
3	4830K241	Standard-Wall Type 304/304L Stainless Steel Thread Pipe Nipple, 1-1/4 Pipe Size X 1-5/8" Length, Fully Threaded	1	4.86	4.86	Double Cone: Male 1.25" to connect to female to female reducer part 4464K539
4	5350K45	Zinc-Plated Steel Barbed Hose Fitting, Standard-Wall Adapter, 3/4" Hose ID X 3/4" NPT Male Pipe	1	4.06	4.06	Double Cone: Hose fitting
5	5231K385	Clear PVC Tubing 3A Sanitary, 3/4" ID, 1" OD, 1/8" Wall Thickness, 10 ft. Length	1	14.9	14.90	Double Cone: Hose to feed thermocouples through

6	44605K313	Low-Pressure Black Malleable Iron Thread Fitting, 3/4 Pipe Size, Adapter, Female X Male	1	7.85	7.85	Double Cone: Female to Male Pipe Fitting
7	5388K24	Worm-Drive Hose Clamp with Zinc Plated Steel Screw, 15/16" to 1-1/2" Clamp Diameter Range, 5/16" Band Width, packs of 10	1	7.37	7.37	To clamp hoses to fitting
				Sum:	**60.06**	

Order on 5/10						
Line	**Product #**	**Product**	**Ordered**	**Price/Each**	**Total**	**Note**
1	5350K48	Zinc-Plated Steel Barbed Hose Fitting High Flow Barbed X Male for 3/4" Hose ID, 1" Pipe	1	6.06	6.06	MSL: hose fitting from sting to hose
2	5350K45	Zinc-Plated Steel Barbed Hose Fitting Std-Wall Adapter, 3/4" Hose ID X 3/4" NPT Male Pipe	1	4.06	4.06	MSL: hose fitting from hose to feed through plate
3	44605K137	Low-Pressure Blk Malleable Iron Thrd Fitting 1-1/4 Pipe, 90 Deg Elbow, Female X Male	2	7.85	15.70	MSL and DC elbow from sting
4	44605K135	Low-Pressure Black Malleable Iron Threaded Fitting, 3/4 Pipe, 90 Degree Elbow, Female x Male	2	3.57	7.14	MSL and DC elbow to feed through plate
5	7767T81	Low-Carbon Steel Tubing 2" OD, 1.250" ID, .375" Wall Thickness, 3' L	1	99.04	99.04	MSL: Sting pipe
6	4830K241	Std-Wall Type 304/304L SS Thrd Pipe Nipple 1-1/4 Pipe Size X 1-5/8" Length, Fully Threaded	1	4.86	4.86	MSL: Male part from elbow to adapter
7	4464K539	Type 304 Stainless STL Threaded Pipe Fitting 1-1/4 X 1 Pipe Size, Reducing Coupling, 150 PSI	1	14.96	14.96	MSL: sting female reduce diameter pipe from 1.25 " to 1"
8	89015K275	Multipurpose 6061 Aluminum, Sheet, .190" Thick, 6" x 6"	1	12.23	12.23	MSL and DC: Thin sheet of aluminum to make feed through plate
9	8924K68	High-Strength 1045 Medium Carbon Steel Rod, 2-1/2" Diameter, 1' Length	1	51.68	51.68	MSL: needed to manufacture the sting

10	90322A146	Grade 8 Steel Fully Threaded Rod, 1/2"-13 Thread, 1-1/2" Long	1	2.88	2.88	MSL: Rod connecting aftbody to mount
11	91251A540	Black-Oxide Alloy Steel Socket Head Cap Screw, 1/4"-20 Thread, 3/4" Length, packs of 50	1	7.20	7.20	MSL: Screws for connecting sting
				Sum:	225.81	

Returns			**Ordered**	**Price/Each**	**Total**	**Note**
Line 2: 04/01	1388K411	Low-Carbon Steel Sheet, 3/4" Thick, 6" X 6", Ground Finish	1	-57.79	-57.79	Unused (originally for flange face)
Line 5: 05/10	7767T81	Low-Carbon Steel Tubing 2" OD, 1.250" ID, .375" Wall Thickness, 3' L	1	-99.04	-99.04	MSL Sting pipe was returned
				Sum:	**-156.83**	

Machine Shop	Hours	Price/Hour	
Double Cone	39	61	2379.00
MSL	22.5	61	1372.50
Total:	**61.5**	**61**	**3751.50**

Total Cost:	**4316.67**